A COMPREHENSIVE APPROACH TO MONITORING VOLCANO DEFORMATION AS A WINDOW ON THE ERUPTION CYCLE

Daniel Dzurisin
David A. Johnston Cascades Volcano Observatory
U. S. Geological Survey
Vancouver, Washington, USA

Received 5 December 2001; revised 21 June 2002; accepted 20 August 2002; published XX Month 2003.

[1] Since the 1980 eruption of Mount St. Helens, volcanologists have made considerable progress toward predicting eruptions on the basis of precursors that typically start a few days to several months in advance. Although accurate eruption prediction is by no means routine, it may now be possible in some cases to extend the effective warning period by anticipating the onset of short-term precursors. Three promising indicators of deep magmatic processes are (1) deep, long-period earthquakes and tremor that indicate the ascent of magma through the crust, (2) magmatic CO_2 emission rate as a proxy for magma supply rate, and (3) relatively broad, generally aseismic surface uplift caused by magmatic intrusions. In the latter case it is essential to sample the deformation field thoroughly in both time and space to adequately constrain source models. Until recently, this has been nearly impossible because high-precision sensors could not be deployed in sufficient numbers, nor could extensive geodetic surveys be conducted often enough. Advances in instrumentation, interferometric synthetic aperture radar (InSAR), and telecommunications are helping to overcome these limitations. As a result, comprehensive geodetic monitoring of selected volcanoes is now feasible. A combination of InSAR, large-aperture GPS surveys, microgravity surveys, and dense arrays of continuous GPS stations, strain meters, and tiltmeters can reveal both spatial and temporal patterns of ground deformation throughout the eruption cycle. Improved geodetic monitoring of many of the world's volcanoes would be a major stride toward better understanding of magmatic processes and longer-term eruption forecasts. *Index Terms:* 8419 Volcanology: Eruption monitoring (7280); 8434 Volcanology: Magma migration; 8494 Volcanology: Instruments and techniques; 8499 Volcanology: General or miscellaneous; *Keywords:* volcano geodesy, volcano deformation, volcano monitoring, radar interferometry

Citation: Dzurisin, D., A Comprehensive Approach to Monitoring Volcano Deformation as a Window on the Eruption Cycle, *Rev. Geophys., 41*(X), XXXX, doi:10.1029/2001RG000107, 2003.

1. INTRODUCTION

1.1. Recent Progress in Volcano Hazards Mitigation

[2] Considerable progress has been made during the past few decades toward understanding volcanic processes and mitigating volcano hazards. There have been significant advances in eruption prediction, hazards assessment, and public education, which together form the basis for improved preparedness and hazards mitigation. Rather than attempting a comprehensive review of these developments, this paper mentions a few recent successes and then focuses on one aspect of volcanology, geodesy, that is providing important new insights into the structure and workings of volcanoes. The examples are U.S. and U.S. Geological Survey (USGS) centric, but much of the discussion is general and hopefully will be of broad interest.

[3] The reawakening of Mount St. Helens, Washington, in 1980 after more than a century of inactivity was correctly forecast a few years in advance based on the volcano's stratigraphic record of past eruptive activity [*Crandell et al.*, 1975; *Crandell and Mullineaux*, 1978]. Starting with the recognition of unusual seismicity beneath Mount St. Helens on 20 March 1980, an intensive monitoring effort revealed patterns of earthquakes, ground deformation, and volcanic gas emissions that prompted public access restrictions and provided the basis for increasingly specific and accurate predictions of six explosive eruptions in 1980 and more than a dozen dome-building episodes during 1980–1986 [*Swanson et al.*, 1983; *Brantley and Myers*, 2000].

[4] The tragic deaths of more than 23,000 people in Armero, Colombia, in 1985 as a result of an eruption-triggered lahar at Nevado del Ruiz volcano underscored the importance of timely and effective communication

Copyright 2003 by the American Geophysical Union.

8755-1209/03/2001RG00010715.00 doi:10.1029/2001RG000107

among scientists, public officials, and the general population [*Voight*, 1996]. Shortly thereafter, the Volcano Disaster Assistance Program (VDAP) was established to reduce losses from future eruptions. VDAP is credited with helping to save tens of thousands of lives during the great 1991 eruption of Mount Pinatubo, Philippines [*Punongpayan et al.*, 1996] and has responded to dozens of other volcano crises worldwide.

[5] More recently, there have been several successful eruption forecasts in the Aleutian volcanic arc, Alaska. Redoubt Volcano produced more than 20 large tephra eruptions and associated pyroclastic flows, lahars, and dome growth during a 6-month period that began on 14 December 1989, following 23 years of quiescence [*Miller and Chouet*, 1994]. The eruptions severely disrupted air traffic [*Casadevall*, 1994] and commerce throughout south central Alaska and caused economic losses estimated >$160 million. On 13 December 1989 the Alaska Volcano Observatory (AVO) announced that an intense swarm of long-period earthquakes beneath Redoubt might soon lead to an eruption. The first two explosive events occurred <24 hours later [*Power et al.*, 1994]. AVO also issued advance warnings of several subsequent eruptions based on precursory long-period seismicity [*Chouet et al.*, 1994].

[6] On 27 June 1992, Crater Peak on the south flank of Mount Spurr erupted after 39 years of inactivity [*Eichelberger et al.*, 1995]. Earlier that month, AVO noted increased seismicity and advised government agencies and the aviation industry to review eruption response plans. Crater Peak erupted again on 18 August and 16–17 September 1992. Both the June and September eruptions were successfully forecast on the basis of precursory seismicity. Although the August event was not forecast, seismic confirmation of the activity allowed AVO to issue an eruption notification within minutes and thus to warn aircraft of the ash hazard [*Power et al.*, 1995].

[7] There have also been helpful responses to seismic crises at other Aleutian volcanoes that did not culminate in eruptions. For example, a swarm of shallow earthquakes beneath Mount Dutton during July–August 1988 was felt sharply in nearby communities, causing much concern. AVO monitored the situation as it developed and reassured residents that an eruption was not imminent, based on the character of seismicity and Dutton's recent eruptive history. A similar occurrence at Akutan Volcano in March 1996 produced a similar outcome. An intense earthquake swarm began on 10 March, causing apprehension in the nearby village of Akutan. At the peak of the swarm, earthquakes were felt every few minutes and >40 events/hour were recorded by seismometers 300 km away. Activity declined temporarily until another intense swarm began on 13 March. Felt earthquakes occurred at the rate of about one per minute, including at least 3 of M 5.0–5.3 [*Lu et al.*, 2000a]. Scientists were on hand to reassure ~1000 residents and avoid an unnecessary evacuation or shutdown of a $10 million/month fish-processing facility. Seismicity eventually returned to background levels without an eruption. Synthetic aperture radar interferograms revealed a complicated pattern of ground deformation across most of Akutan Island, which *Lu et al.* [2000a] modeled as inflation of an ~13 km-deep magma body beneath the volcano's west flank and propagation of a dike to within 1 km of the surface.

1.2. New Challenges Include Earlier Recognition of Volcanic Unrest

[8] Despite such progress many eruptions around the world still come as a surprise to people living near the volcano. The reasons are undoubtedly varied and complex, but an important factor in many cases is that dangerous volcanoes tend to erupt infrequently. A time span of several generations, though fleeting by geologic standards, is long enough for social memory of an eruption to fade to the extent that a once dangerous volcano becomes a friendly mountain in the minds of living residents. This was the case at Mount St. Helens prior to 1980, El Chichón (Mexico) prior to 1982, and Mount Pinatubo prior to 1991, where devastating eruptions were preceded by reposes of 123 years, ~600 years, and ~500 years, respectively, and many residents were unaware of the hazards before their "mountain" began to rumble.

[9] Of course, volcanologists are more aware of the geologic past than most of the population, but they, too, are often surprised by the start of volcanic unrest. In this case it is not the volcanic nature of the activity that comes as a surprise but rather its specific timing. Even in hindsight, there were no recognizable signs that Mount St. Helens was about to reawaken prior to the first shallow earthquakes beneath the volcano in March 1980. The 2-month precursory period leading up to the climactic eruption on 18 May 1980 represents only ~0.1% of the 123-year repose interval since the end of the previous eruption. What happened beneath Mount St. Helens during the preceding 99.9% of its repose? Could volcanologists have known before March 1980 that the volcano was about to reawaken?

[10] Conceptually, the eruption cycle is a continuum from deep magma generation through surface eruption, including such intermediate stages as partial melting, initial ascent, crustal assimilation, magma mixing, storage, degassing, partial crystallization, and final ascent to the surface. Not all stages are represented in every event. For example, some eruptions are fed from shallow magma bodies that might not be replenished before every eruption, and others produce primitive lavas that show no evidence of storage, assimilation, or mixing. The timescale for magma generation, ascent, and storage is poorly constrained and variable from one eruption to the next. In some cases the early part of the cycle is relatively brief (e.g., rapid ascent of magma from a deep source directly to the surface), or the latter part is protracted (e.g., long periods of storage, assimilation,

and crystallization between eruptions of large silicic caldera systems). Such complexities notwithstanding, eruptions are the culminating stage of a process that starts deep within the Earth and goes mostly unnoticed until magma is very near the surface.

[11] An alternative point of view deserves consideration here: Eruptions might be caused by sporadic injections of magma that occur with random vigor and hence to random stagnation levels, which in some cases exceed zero depth. If so, a given intrusion says nothing about the next one. Accordingly, "eruption cycle" is a much narrower concept than suggested above (i.e., each intrusion is a separate cycle that produces either an eruption or a "failed eruption"). In either case, unrest is typically recognized only very late in a sequence of events that includes (at least) magma generation and ascent through the crust. Whether eruptions are random events fed by single intrusions or culminations of multiple intrusions that forge a passageway and supply a long-lived magma reservoir, it might be possible with new techniques to detect such occurrences earlier and thus to provide longer-term warnings. That said, the possibility is acknowledged that failed eruptions might have little to do with the next event at the same volcano, and the reader should keep this in mind for what follows.

[12] The absence of measurable precursors until late in the eruption cycle, when magma begins its final ascent, is mainly a consequence of three factors: (1) The brittle-ductile transition is relatively shallow beneath most volcanoes (typically ~5 km) [*Hill*, 1993], so the slow ascent of magma to that depth is generally not marked by short-period earthquakes (the 1990–1995 eruption of Unzen, Japan, may be a counterexample [see *Nakada et al*., 1999a]); (2) very few volcanoes are monitored well enough to detect long-term changes in the types and amounts of volcanic gases emitted over time, which might signal the ascent of magma from greater depth; and (3) most classical geodetic techniques are not sensitive enough to detect subtle ground deformation that might occur when magma accumulates near the brittle-ductile transition, especially if the intrusion occurs gradually or episodically in a series of small events. Therefore a breakthrough in the ability to predict the onset of volcanic unrest might require a significant advance in volcano seismology, gas geochemistry, or geodesy.

[13] The detection of long-period earthquakes at mid-crustal depths beneath Long Valley caldera, California [*Hill and Pitt*, 1992; *Pitt and Hill*, 1994], Kilauea volcano, Hawaii [*Warren et al*., 1997], and elsewhere is promising, because such events are direct indicators of rising magma [*White and Dzurisin*, 1997]. Likewise CO_2 emission rate may serve as a proxy for magma supply rate, at least at oceanic hot spot volcanoes like Kilauea [*McGee et al*., 2000; *Gerlach et al*., 2002], and thus indicate which volcanoes are likely to reawaken soon.

[14] There have been promising developments in volcano geodesy as well. With a combination of satellite surveillance, repeated surveys, and continuous monitoring, it is now possible to measure ground deformation over very broad areas and with extremely fine temporal and spatial resolution. The next step is to formulate a strategy for monitoring deformation at volcanoes where magma might be accumulating aseismically to test the hypothesis that short-term eruption precursors are preceded by deeper and therefore subtle changes that, nonetheless, can be measured at the surface. This paper develops a rationale for comprehensive geodetic monitoring at volcanoes and invites a dialogue on the future of volcano geodesy.

2. GLIMPSES OF THE ERUPTION CYCLE FROM RADAR INTERFEROMETRY AND BOREHOLE STRAIN METERS

[15] Most arc volcanoes seem to spend most of their time doing little or nothing at all. For example, in a typical year Mount Rainier produces just a few dozen small, shallow earthquakes, a few of them in minor flurries, that *Moran et al*. [2000] attribute to stresses associated with the circulation of hot fluids. No ground deformation has been detected by repeated electronic distance-measuring instrument (EDM) surveys, and emissions of magmatic SO_2 and CO_2 are below detection thresholds. The volcano has erupted several times in the past 1000 years, most recently in the mid nineteenth century [*Crandell*, 1971], but there is no indication from more than 2 decades of monitoring that the volcano is any closer to its next eruption. Present-day quiescence notwithstanding, Mount Rainier will surely "turn on" again someday, much like Mount St. Helens did on 20 March 1980. The same can generally be said for Mount Hood, Mount Shasta, and other Cascade volcanoes. Each day brings us closer to the next eruption, but there is no clue from monitoring as to when or where it will happen. A ticking clock is the best measure we have of the advancing eruption cycle.

2.1. Hints of Early Precursors From Interferometric Synthetic Aperture radar (InSAR): A Remarkable Geodetic Imaging Tool

[16] Recently, InSAR has shed some light on what arc volcanoes do when they are not erupting. The answer has positive implications for extended eruption forecasting (i.e., for anticipating the end of volcanic quiescence). Two examples serve to illustrate InSAR's potential. First, *Lu et al*. [2000b] produced several interferograms from ERS-1 and ERS-2 radar images of Westdahl, an active shield volcano located on Unimak Island in the central Aleutian arc. They showed that the summit area rose ~17 cm from 1993 to 1998 (Figure 1) and that the inflation rate was not steady (i.e., more inflation occurred from 1993 to 1995 than from 1995 to 1998). A best fit elastic model of the deformation indicated that a source 9 km beneath the center of the volcano inflated

by 0.05 km^3 from 1993 to 1998. We know from experience elsewhere that active shield volcanoes inflate episodically between eruptions (e.g., Kilauea, Krafla, and Piton de la Fournaise), so at first glance the Westdahl result is not surprising. However, the source is deep relative to most active shields, where source depths are typically 3–5 km, and the Westdahl inflation was not accompanied by any unusual seismicity. Prior to 1998, the closest seismometers were located 170 km ENE of Westdahl, so local earthquakes smaller than $M \sim 2.5$ could have gone undetected. Nonetheless, inflation of shallow magma reservoirs is often accompanied by increased seismicity, including earthquakes large enough to have been detected if they had they occurred beneath Westdahl prior to 1998. Since a local seismic network was installed at Westdahl in 1998, the level of seismicity has been low.

[17] A more striking result with broader implications for the eruption cycle at arc volcanoes comes from Mount Peulik, a small stratovolcano that partially overlaps the north flank of Ugashik caldera on the Alaska Peninsula, ~550 km southwest of Anchorage [*Miller et al.*, 1998]. There are only two reports of historical activity at Mount Peulik, in 1814 and 1852 [*Doroshin*, 1870]. No fumarolic activity was noted when the summit dome was examined in 1973 [*Miller et al.*, 1998], and no unusual activity of any kind had been noted in the area since the formation of Ukinrek Maars, ~15 km northwest of Peulik, in 1977. In short, the volcano had been quiet for almost 150 years, and there was no indication when it might reawaken.

[18] An intense earthquake swarm, including three M_L 4.8–5.2 events, occurred near Becharof Lake, 30 km northwest of Peulik, from May to October 1998. All of the earthquakes were at least 15 km from Peulik, but radar interferograms showed progressive inflation of the volcano from October 1996 to September 1998 [*Lu et al.*, 2002a] (Figure 2). A presumed magma body located 6.6 ± 0.5 km beneath the southwest flank of Peulik inflated 0.051 ± 0.005 km^3 during that interval. The average inflation rate was 0.003 km^3/month from October 1996 to September 1997, it peaked at 0.005 km^3/month from 26 June to 9 October 1997, and it dropped to 0.001 km^3/month from October 1997 to September 1998. By May 2001 the volcano had returned to quiescence.

[19] The Mount Peulik results are important for at least three reasons. First, they demonstrate that long-quiescent but still active stratovolcanoes inflate episod-

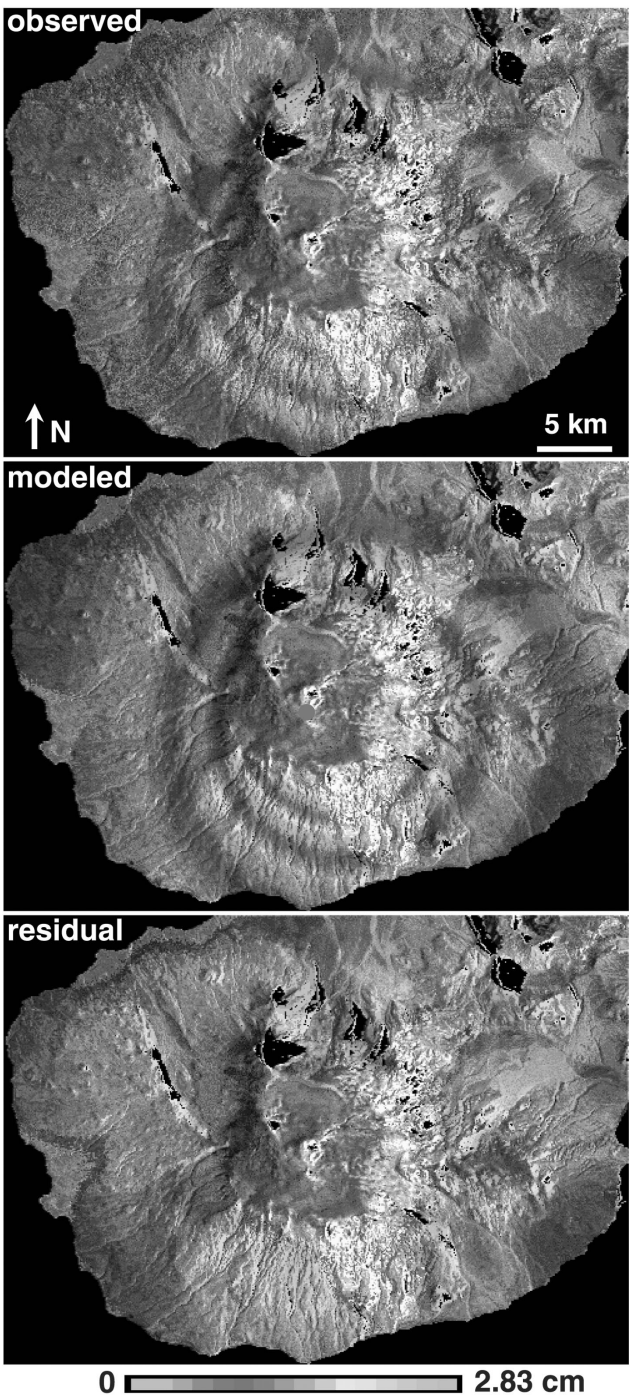

Figure 1. Observed, modeled, and residual interferograms of Westdahl volcano, Alaska, spanning the time interval from 21 September 1993 to 9 October 1998. *Lu et al.* [2000b] produced several such interferograms from pairs of radar images acquired by the European Space Agency's ERS-1 and ERS-2 satellites and a U.S. Geological Survey (USGS) digital elevation model (DEM). Color bands represent interferometric fringes; each full color cycle corresponds to 2.83 cm of range change between the ground and satellite. About three fringes are visible on the volcano's southwest flank. Uncolored area near summit represents permanent ice and snow, where interferometric synthetic aperture radar (InSAR) is ineffective. Extrapolation of the modeled interferogram indicates that the summit moved toward the satellite (i.e., mostly upward because the satellite look angle is ~21° from vertical) ~17 cm during the 5-year observation interval, which did not include any unusual seismicity. *Lu et al.* [2000b] attributed the deformation to magmatic inflation ($\Delta V \approx 0.05$ km^3) of a source ~9 km beneath the center of the volcano (red dot in middle image). See color version of this figure at back of this issue.

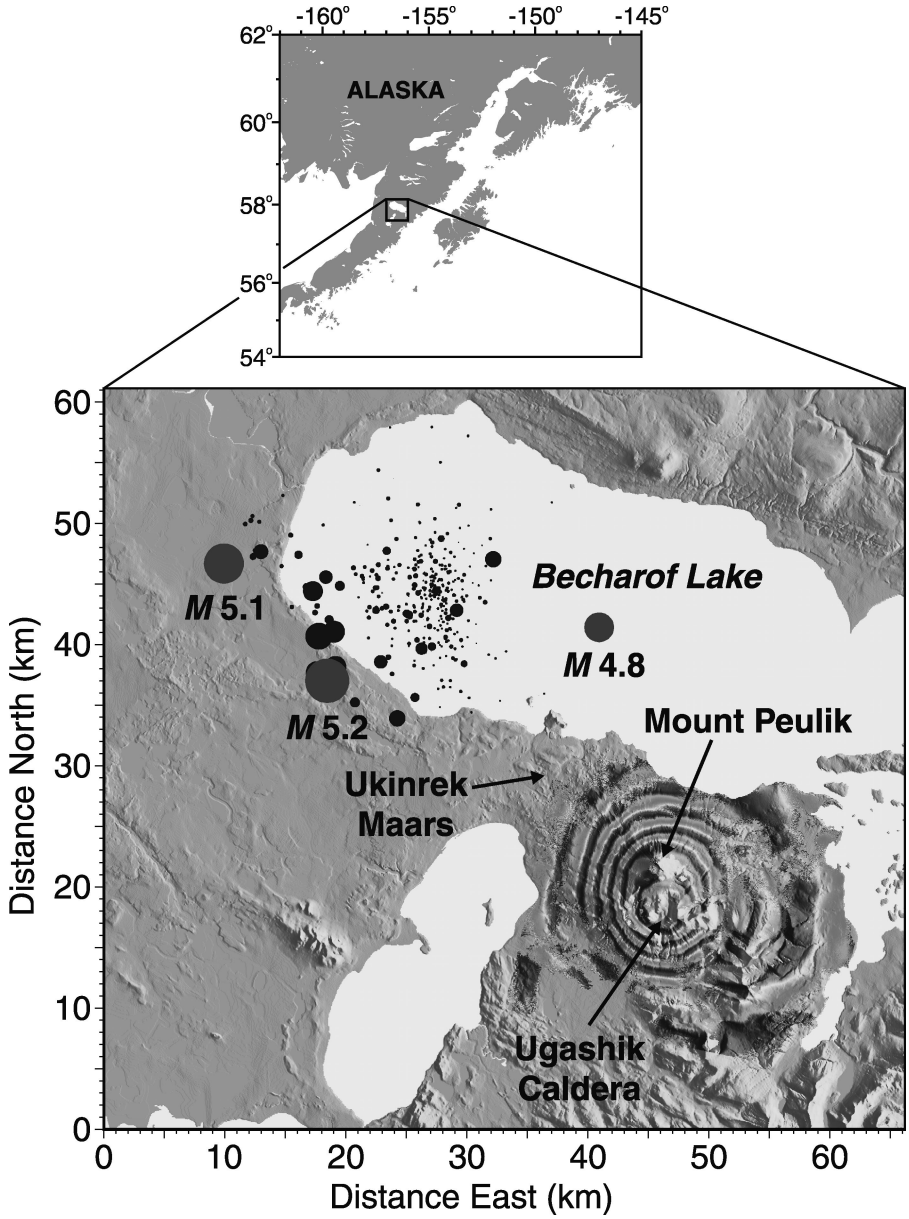

Figure 2. Shaded relief map of the area near Mount Peulik volcano, Alaska, based on the USGS 15-min Alaska DEM. Superimposed on the topography is a radar interferogram for the period from October 1996 to September 1997, showing ~17 cm of inflation centered beneath the volcano's southwest flank. Each interferometric fringe (full color cycle) represents 2.83 cm of range change between the ground and the satellite. Uncolored areas indicate vegetation or other factors that render InSAR ineffective. *Lu et al.* [2002a] used several such interferograms to show that the average inflation rate was ~0.003 km^3/month from October 1996 to September 1997, that it peaked at 0.005 km^3/month from 26 June to 9 October 1997, and that it dropped to 0.001 km^3/month from October 1997 to September 1998. No unusual seismicity was detected beneath the volcano during the inflation episode. However, an intense earthquake swarm occurred ~30 km northwest of Mount Peulik, in the vicinity of the southwest shoreline of Becharof Lake, from May to October 1998. Black ($M < 4.8$) and red ($4.8 \leq M \leq 5.1$) circles represent epicenters of the 1998 swarm. The smallest circles correspond to $M = 0$ and the largest to $M = 5.2$. *Lu et al.* [2002a] modeled the deformation as inflation ($\Delta V = 0.051 \pm 0.005$ km^3) of a magma body located 6.6 ± 0.5 km beneath the southwest flank of Mount Peulik. See color version of this figure at back of this issue.

ically during repose; centuries-long eruption cycles might include many such episodes. Second, the temporal and spatial relationships between the 1998 Becharof Lake earthquake swarm and the 1996–1998 Peulik inflation episode hint at a poorly understood link between magmatic and tectonic processes. *Lu et al.* [2002a] explored the possibility that the swarm was triggered by Coulomb stress changes in the epicentral area caused by magma intrusion beneath the volcano and showed that the changes were of the right sign but probably too small

(<0.1 bar). Finally, the Peulik results are important because they demonstrate that InSAR can successfully image surface deformation caused by magma recharge episodes that might otherwise go undetected.

2.2. Late-Stage Geodetic Precursors From Borehole Strain Meters: Continuous Sensors With Unmatched Sensitivity to Crustal Strain

[20] Another rich source of information about how magma moves through the crust, in this case during the final minutes before erupting, comes from an array of borehole strain meters near Hekla Volcano, Iceland. When well coupled to rock 100–200 m beneath the surface, the Sacks-Evertson strain meter [*Sacks et al.*, 1971] has sensitivity to dilatational strain of the order of 10^{-12} over periods of seconds to minutes and is capable of resolving strain changes of 5×10^{-9} over periods of a few hours to a few days and strain changes of 5×10^{-8} over periods of months [*Johnston et al.*, 1994]. Fortuitously, five of these instruments were installed at sites 15–45 km from Hekla in 1979 to monitor a region of high seismic potential [*Linde et al.*, 1993]. All five recorded strain changes were associated with explosive eruptions of Hekla in January 1991 and February–March 2000.

[21] Recognized geodetic precursors to the 1991 Hekla eruption were remarkably brief. Anomalous strain changes began shortly after 1630 local time on 17 January only ~30 min before the inferred start of the eruption at 1701 [*Linde et al.*, 1993]. A two-stage model reproduces the strain meter data very well. In stage 1, magma moved out of a 6.5-km-deep reservoir and into a dike that migrated to the surface at an average rate of 10–15 km/h. During stage 2, which started when the dike reached the surface, the reservoir continued to deflate for 2 days while the eruption ran its course. According to the model, 0.1 km^3 of magma moved out of the reservoir, in good agreement with the volume of material erupted.

[22] A similar pattern of strain changes accompanied the February–March 2000 eruption [*Linde and Sacks*, 2000], which was predicted with remarkable accuracy on the basis of precursory seismicity and strain changes [*Agustsson et al.*, 2000]. At 1700 local time on 26 February 2000, a seismometer within 2 km of the summit began recording a sequence of small earthquakes ($M <$ 1), which are rare at Hekla except as a prelude to eruptions. As the swarm intensified, the Civil Defense of Iceland was warned at ~1715 of an imminent eruption. At 1747 a Sacks-Evertson borehole strain meter 15 km from Hekla started recording increasing contraction. On that basis a prediction was issued to the Civil Defense at 1753 stating that an eruption was to be expected within 15–20 min and recommending that a public warning be issued. The warning was broadcast immediately, and Hekla began erupting explosively at 1817.

[23] The apparent lack of longer-term strain precursors to the Hekla eruptions is surprising. The data indicate that 0.1 km^3 of magma accumulated in a reservoir 6.5 km beneath the volcano without causing any measurable strain near the surface, even at the closest strain meter 15 km away. This result is contrary to a simple elastic model unless (1) the magma arrived too slowly to be detected by the strain meters, (2) the magma arrived before the strain meters were installed, (3) simultaneous draining of a deeper magma storage zone masked the effects of shallow inflation, or (4) the brittle-ductile transition beneath Hekla is shallow enough to strongly attenuate elastic strain at 6–7 km depth, thus depriving the strain meters of longer-term precursors.

2.3. Longer-Term Precursory Strain Indicated by Water Level Changes

[24] Not all geodetic precursors to explosive eruptions are so brief. The 2000 eruption of Usu Volcano, Japan, which followed 23 years of dormancy, was preceded by several months of systematic water level changes in two wells within 1 km of the vent [*Shibata and Akita*, 2001]. In early October 1999 the residual water level (corrected for barometric pressure, Earth tides, and the influence of nearby Lake Toya) in the 115-m-deep T10 well started to drop at a rate of 0.18 m/month. Starting in January 2000, the rate increased to a peak of 0.38 m/month, resulting in a total drop of 1.5 m before the start of the eruption on 31 March 2000. At the nearby 1200-m-deep GSH-1 well the residual water level increased by 0.05 m from 31 December 1999 to 3 January 2000 then gradually decreased by 0.02 m/month before suddenly dropping more than 5 m on 28 March 2000. The level rose again until water spouted from the well like a fountain on 3 April 2000, 3 days after the start of the eruption. The 0.5-m-rise in water level at GSH-1 corresponds to $7.4–7.7 \times 10^{-8}$ contractional strain.

[25] *Shibata and Akita* [2001] interpreted these remarkable changes as follows: (1) Water migrated into fractures that were gradually intruded and widened by magma, causing the water level in T10 to drop starting in October 1999; (2) from 31 December 1999 to 3 January 2000, volumetric expansion of a magma reservoir beneath Usu compressed the overlying crust, causing the initial water level rise at GSH-1; (3) water continued to flow into fractures as the dike expanded, causing the water level to start dropping at GSH-1 and to drop more rapidly at T10; (4) a few days before the eruption, the dike's final ascent to the surface was heralded by a swarm of shallow volcanic earthquakes and a precipitous drop in water level at GSH-1; and (5) the rapid rise in water level and spouting from GSH-1 3 days after the eruption might have been caused by injection of thermal fluid or pressurized gas from the intrusion.

[26] The InSAR, strain meter, and water well results described above seem to pose a paradox. On the one hand, InSAR has detected aseismic uplift of quiescent volcanoes that suggests either progressive (Westdahl) or episodic (Peulik) magma recharge of midcrustal reservoirs between eruptions, and water level changes near

Usu have indicated precursory strain up to 6 months prior to the 2000 eruption. On the other hand, the Hekla strain meters measured no precursory strain associated with a 6.5-km-deep reservoir until just ~30 min before the 1991 and 2000 eruptions. Would InSAR or water wells have detected inflation of the Hekla reservoir months to years before those eruptions? Or is Hekla fundamentally different in this regard, perhaps because of its setting on oceanic crust? If magma accumulation beneath volcanoes can be detected geodetically months or years before an eruption, meaningful steps can be taken to mitigate the eruption's social and economic impact. However, if significant volumes of magma can accumulate in the crust and escape detection, even by extremely sensitive borehole strain meters, until less than an hour before erupting, longer-term hazards mitigation will be much more difficult. To determine which of these two scenarios is more realistic, a diverse set of volcanoes would have to be monitored comprehensively throughout one or more eruption cycles. "Comprehensively" implies both spatial and temporal completeness, plus adequate sensitivity to resolve geodetic signals from relatively small-volume ($\leq$0.1 km^3) or deep ($\geq$5 km) intrusions.

2.4. Current State of Knowledge: Diversity, Complexity, and Opportunity

[27] Available InSAR and strain meter results hint at considerable diversity and complexity in the eruption cycles of various volcanoes. For example, InSAR results from several Aleutian volcanoes reveal distinctive deformation patterns that differ in both space and time. At Okmok Volcano, at least 3 years of preeruptive inflation (1992–1995) was followed by coeruptive deflation (1995–1997) and then by at least one year of post-eruptive reinflation (1997–1998) [*Lu et al.*, 2000c]. No InSAR data are available before the 1991–1992 Westdahl eruption, but successive interferograms show that the volcano reinflated for at least 5 years immediately afterward [*Lu et al.*, 2000b]. The inflation rate slowed before the Okmok eruption and after the Westdahl eruption, suggesting that the magma supply rate to these two volcanoes is greatest soon after eruptions and gradually slows thereafter. A similar pattern is well documented by geodetic measurements at Kilauea and Krafla and can be explained by the increased pressure gradient between mantle source regions and shallow magma storage zones resulting from eruptions [*Tryggvason*, 1986; *Dvorak and Okamura*, 1987; *Ewart et al.*, 1991]. One difference between Okmok and Westdahl is that the magma reservoir at Okmok is only ~3 km deep, whereas the Westdahl reservoir is ~9 km deep. At Makushin, a frequently active stratovolcano in the central Aleutians, a small explosive eruption in 1995 was preceded by up to 2 years of inflation but was not clearly accompanied or followed by deflation (perhaps because the volume erupted was very small). A best fit model based on InSAR results places the source ~7 km beneath the volcano [*Lu et al.*, 2002b], intermediate between the results for Okmok and Westdahl.

[28] Further complicating the situation, InSAR has shown that some Aleutian volcanoes deform without erupting (e.g., Akutan in 1996), and others erupt without deforming. Shishaldin erupted repeatedly during 1995–1996 and 1999, but no deformation is recorded by interferograms that span the activity (Z. Lu, personal communication, 2001). Other examples of erupting volcanoes that show little or no deformation in interferograms include [*Zebker et al.*, 2000] Irruputuncu (Chile), Popocatepetl (Mexico), Pacaya and Fuego (Guatemala), Sakurajima (Japan), and Pavlof and Shishaldin (Alaska). The absence of deformation associated with eruptive activity probably has several explanations. Some frequently active volcanoes may be open-vent systems where magma rises through established conduits without causing much strain. In other cases, deformation associated with small eruptions might be too small to measure with InSAR, or preeruptive inflation might be masked by coeruptive deflation. The important point here is that deformation is a complex and therefore rich source of information about subvolcanic conditions and processes. The challenge is to extract as much of the information as possible with limited resources, a task that requires state-of-the-art monitoring and modeling techniques.

3. GUIDANCE FROM NUMERICAL MODELING

[29] If we accept the possibility that, even during repose, volcanoes do interesting things that might cause measurable surface deformation, how should we design a monitoring strategy to capture as much of the geodetic signal as possible? Specifically, what measurements should we make, where, and how often? *Dzurisin* [2000] pointed out that volcano deformation, especially during long repose periods, can be very elusive. For example, a brief episode of reversible deformation might be missed entirely by infrequent surveys. Such surveys would presumably detect permanent deformation if it were large enough, but the time history (i.e., steady or episodic) would not be well determined. Surveys of a small, dense geodetic network might underestimate deformation caused by a deep source, while surveys of a broad, sparse network might miss the effects of a shallow source entirely. Such difficulties can be partly overcome by using continuous sensors such as continuous GPS (CGPS), strain meters, or tiltmeters. However, the location of continuous sensors is critically important. For example, if all sensors are located too close to the center of deformation, it might not be possible to distinguish between an inflating dike and a deflating sphere, which both produce localized subsidence. Even a dense array of sensors close to a volcano might not detect broad, subtle uplift caused by inflation of a relatively deep source. Conversely, an extensive but sparse array of

sensors might fail to record localized deformation caused by a shallow source. *Dzurisin* [2000, p. 1564] discussed these complexities and concluded "… to distinguish among the full range of possible source locations and geometries, especially if multiple sources might be present, it is necessary to make measurements virtually 'everywhere, all the time'"; this an impractical but worthwhile goal.

[30] The need for a comprehensive approach to monitoring is illustrated by results from numerical modeling, which show that the deformation field can be complex and difficult to interpret without a very detailed set of geodetic measurements. From the geodetic data we would like to determine the location, geometry, and strength of all sources that might influence the behavior of a volcano. This is an intractable inverse problem unless the data are spatially dense and extensive enough to provide the necessary constraints. For example, consider just the possibilities for source geometry. Plausible subvolcanic sources include a sphere or "point source" [*Mogi*, 1958; *McTigue*, 1987], triaxial ellipsoid [*Davis*, 1986], closed vertical pipe [*Bonaccorso and Davis*, 1999], dike, sill, and fault dislocation [*Okada*, 1985, 1992]. A complete description of any one source can require as many as nine parameters: three spatial coordinates (x, y, and z), five geometric properties (e.g., length, height, width, dip, and strike for a dike), and one strength parameter (e.g., volume change or fault displacement). Especially for multiple sources, the solution is almost always underdetermined by data. The traditional approach to this problem has been to make various assumptions about the source(s): typically, that it is located beneath the volcano and can be represented as a Mogi source. Such assumptions might compromise the understanding of volcanic processes and therefore should be avoided whenever possible. A robust solution to the inverse problem for multiple sources is an implicit goal of any comprehensive monitoring strategy.

[31] Useful insight into the proper design of geodetic networks at volcanoes can be gained by comparing the deformation fields from two hypothetical sources, a Mogi source and a closed vertical pipe, assuming the crust behaves like a homogeneous, elastic half-space. Model parameters are chosen to approximate those inferred for the magma body that fed the 18 May 1980 eruption of Mount St. Helens [*Scandone and Malone*, 1985]. The Mogi source is modeled as a sphere with a radius of 595 m centered at 9 km depth; the pipe extends from 6.5 to 11 km depth and has a radius of 250 m (Figure 3). The initial volume of both sources is 0.88 km^3, and both volumes are assumed to increase by 0.018 km^3. The resulting patterns of surface displacement, dilatation, and tilt are shown in Figure 4. Details of the models are unimportant as long as the assumed values for volume change and source depth are reasonable. Eruptions with 0.018 km^3 or more of eruptive products occur worldwide at an average rate of several per year [*Simkin and Siebert*, 1994, p. 28–30], which suggests that

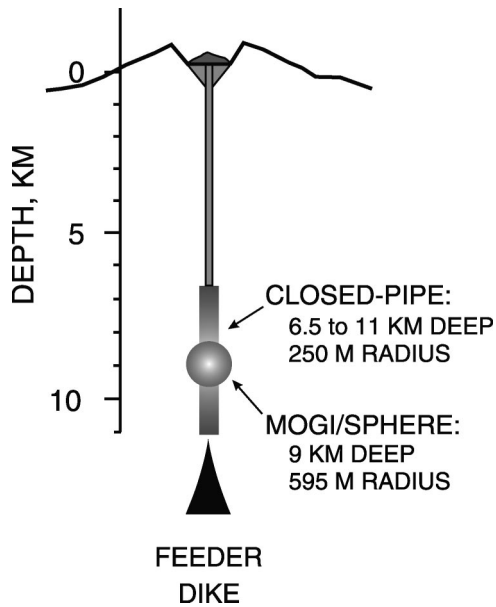

Figure 3. Cross-sectional view of two deformation sources used to model surface deformation: (1) a Mogi source at 9 km depth and (2) a closed pipe extending from 6.5 to 11 km depth. The radii of the sources were chosen to make their volumes equal (V = 0.88 km^3). The surrounding crust was assumed to be elastic and homogeneous. Figure 4 shows calculated surface displacements and strains caused by a volume change of 0.018 km^3 in each source. See color version of this figure at back of this issue.

comparable volume changes beneath volcanoes are not uncommon. Likewise, most models based on volcano deformation data indicate source depths of <10 km (typically 3–6 km), so the 9-km-depth used here is reasonable and probably errs on the side of underestimating the maximum surface deformation.

[32] The main points of Figure 4 are the following: (1) Predicted surface displacements, tilts, and dilatation are easily measurable with modern geodetic techniques, (2) the deformation field is large enough to extend in many cases well beyond the boundary of the volcanic edifice (i.e., >20 km for a 9-km source depth), and (3) deformation patterns for Mogi and pipe sources differ considerably, but distinguishing between these sources (and other possibilities) on the basis of geodetic data is possible only if the differences are clearly reflected in the data. On the last point, consider the model results for vertical displacement (Figure 4, top left). The uplift patterns produced by an inflating Mogi source and a closed pipe are very different in proximal areas (i.e., within ~1/2 source depth) but not in distal areas. The same can be said for dilatation (Figure 4, bottom right). Radial displacement is a relatively poor discriminator between a Mogi source and a closed pipe, while tilt is a relatively good discriminator if data are available in proximal areas. Accordingly, (1) modern geodetic techniques have the potential to reveal the depth, location, and shape of volcano deformation sources; (2) geodetic networks at volcanoes should be broad enough (aperture

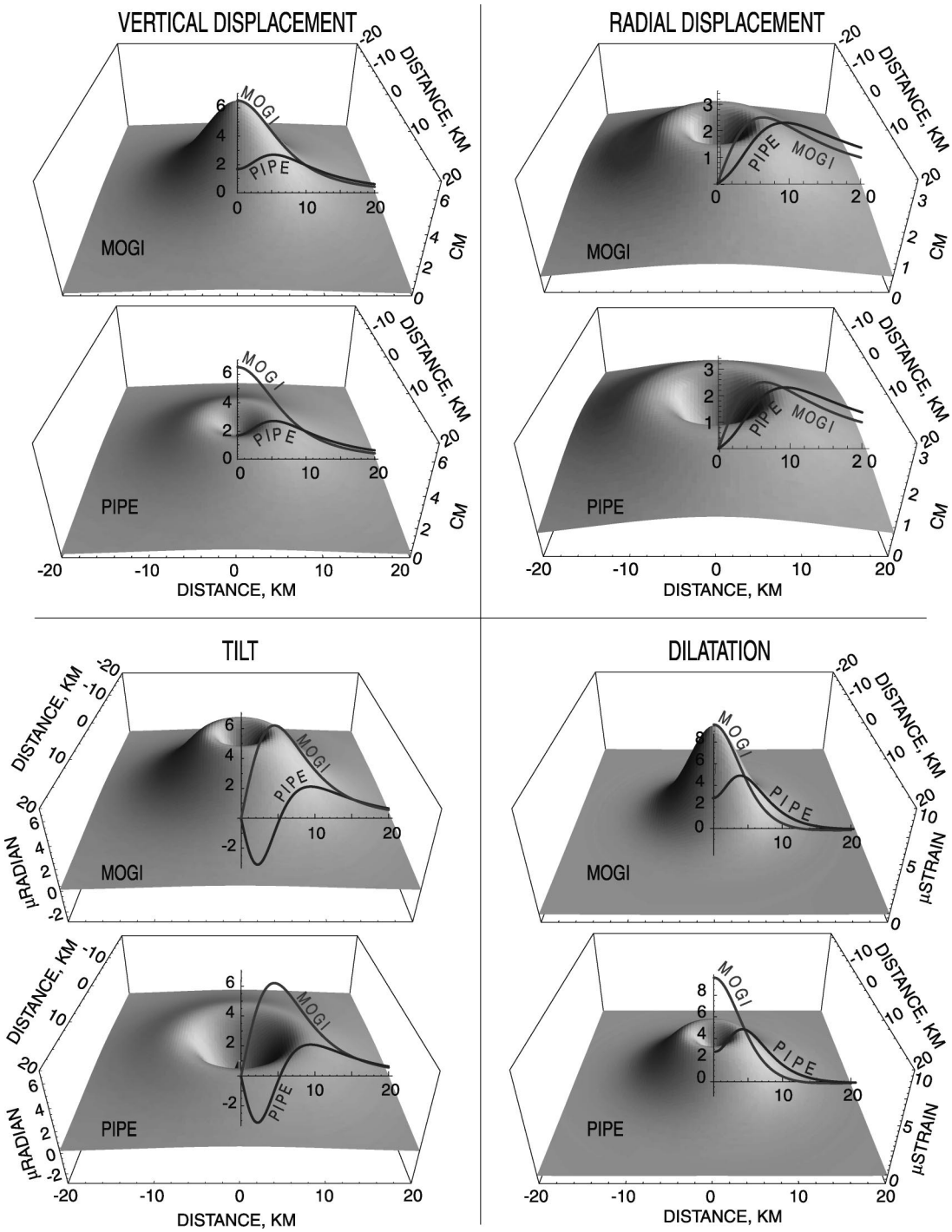

Figure 4. Comparison of model results for a *Mogi* [1958] source centered at 9 km depth and a closed pipe source [*Bonaccorso and Davis*, 1999] between 6.5 and 11 km depth (see Figure 3). Model parameters were chosen to approximate the inferred source for the 18 May 1980 eruption of Mount St. Helens [*Scandone and Malone*, 1985]. Each source has an initial volume of 0.88 km^3 and undergoes a volume increase of 0.018 km^3. Several geodetic sensors at various distances would be required to distinguish between these sources, and the situation would be more complicated if other source geometries were considered (e.g., triaxial ellipsoid, dike, sill, and fault dislocation) or if there were multiple sources, the source depth(s) were not known, or the deformation were not radially symmetric. Numerical modeling and graphic are by E. Roeloffs and M. Lisowski (personal communication, 2001). See color version of this figure at back of this issue.

>20 km) and dense enough in both proximal and distal areas to distinguish among plausible source types and locations; and (3) a comprehensive volcano geodesy program should include complementary techniques and sensors, including both survey and continuous GPS, leveling (where practical), tiltmeters, strain meters, and InSAR.

[33] Departures from elastic behavior (e.g., viscoelastic, plastic, and Coulomb) undoubtedly occur beneath volcanoes, complicating the relationship between subsurface volume changes and surface deformation. For simplicity, this discussion assumes that deformation in response to magma intrusion is purely elastic. This approach hopefully provides some useful guidance and a valid starting point for more thorough treatments of specific volcanic systems.

3.1. Implications for Various Sensor Types and Monitoring Techniques

[34] Imagine that our goal is to determine the depth, size, and shape of a subvolcanic magma body as a function of time. This requires adequate characterization of the resulting surface deformation field to the extent that geodetic data can be inverted to produce a realistic source model. We can see from Figure 4 that, for both source types, relatively large displacements and strains extend outward to approximately one source depth (~10 km), smaller but still measurable effects extend to more than two source depths (>20 km), and within one source depth the deformation field can be relatively complicated (distance is measured at the surface radially outward from the point directly above the source). Accordingly, to achieve our goal we need at least one sensor (preferably three) within ~10 km of the volcano and at least one (preferably two) at 10–20 km. Given that the deformation field might not be radially symmetric, as would be the case if a shear dislocation (fault) or a planar volume source (dike or sill) were added, it would be prudent to install two to five sensors in each quadrant around the volcano, a total deployment of 8–20 sensors. Any smaller number would risk mischaracterization of the deformation field and misleading model results. Details of the deployment would depend on the sensor type, resources available, and logistical considerations. Ideally, how many and what types of sensors should be used?

3.2. Continuous GPS Stations

[35] Figure 4 shows that the calculated vertical displacements for spherical and pipe sources reach their maxima of 3–6 cm at distances of 0–5 km from the volcano and that the amount of uplift is ~2 cm at 10 km and ~0.5 cm at 20 km from the volcano. The maximum radial displacement is smaller by a factor of ~2 for the Mogi source, but radial displacements exceed 1 cm for both sources even at a distance of 20 km. Given the greater sensitivity of GPS to horizontal motion, the calculated vertical and radial displacements should be resolvable by CGPS out to distances of at least 10 km and 20 km, respectively, in a matter of days to weeks. An effective deployment might include, in each quadrant, three CGPS stations within 10 km of the volcano (preferably two within 5 km) and two stations at 10–20 km for a total of 20 stations.

3.3. Borehole Strain Meters

[36] Two other important considerations in designing a geodetic monitoring strategy are instrumental sensitivity to very small strains and the minimum sampling frequency required to adequately record short-term changes, factors that favor borehole strain meters and tiltmeters over CGPS stations. The models represented in Figure 4 indicate that large strains (up to 10 μstrain and 6 μrad) occur within a few kilometers, and measurable strains extend outward beyond two source depths (>20 km in this case). Recall that the Sacks-Evertson strain meter can resolve changes as small as 0.005 μstrain over periods of a few hours to days, a threshold that would be reached well beyond 20 km according to the models. Another very responsive borehole sensor suitable for monitoring volcano deformation is the Gladwin tensor strain meter [*Gladwin*, 1984; *Gladwin and Hart*, 1985]. Unlike the Sacks-Evertson instrument, which measures volumetric strain (a scalar quantity), the Gladwin tensor strain meter measures three independent components of the tensor strain field (ε_{xx}, ε_{yy}, and ε_{xy}). A general three-dimensional strain tensor has six independent components, but near the surface the vertical stress is zero, so the strain field is completely described by these three horizontal components. Strain sensitivity of the Gladwin instrument is of the order of 10^{-11}, and its frequency response is flat from DC to 100 Hz, so it is equally well suited to measuring gradual strain, such as might be caused by magma pressurization and dynamic strains associated with volcanic earthquakes and fluid flow, for example. Both the Sacks-Evertson and Gladwin strain meters are being considered for deployment as part of the Plate Boundary Observatory, a proposal that would include ~150 strain meters and 750 CGPS stations across the western United States, including clusters near selected volcanoes in the Aleutians and Cascades, Long Valley, and Yellowstone.

[37] A comprehensive geodetic monitoring program should include at least one borehole strain meter as close to a volcano's summit as practical and at least one (preferably two) in each quadrant within 10 km of the summit. As with all continuous sensor types, details of the network design might be influenced by such local factors as faults or logistical considerations. As demonstrated at Hekla, additional strain meters 10–50 km from the volcano could also be very valuable. Borehole strain meter installations are relatively difficult and expensive, so in many cases the minimum number (five) might be a practical limit. Nonetheless, more is clearly better.

3.4. Tiltmeters

[38] A final consideration based on the modeling results is that ground tilt in proximal areas is a very good indicator of source geometry. Notice in Figure 4 that the tilt patterns within 10 km of the source are distinctly different for the Mogi and pipe sources. In some cases the calculated tilts are even of opposite sign. Also, tilt-

meters offer important logistical advantages over other types of continuous sensors. Tiltmeters generally require less power than GPS receivers or strain meters and therefore are easier to maintain in remote areas and in harsh climates. Installing tiltmeters in boreholes or tunnels generally produces substantial improvement in the signal-to-noise ratio relative to near-surface installations, because the amplitude of background noise attenuates strongly with depth. For signals with periods of days to months an order of magnitude improvement is attainable at 30 m depth and 2 orders of magnitude is attainable at 200 m depth [*Johnston and Borcherdt*, 1984; *Johnston et al*., 1986; *Johnston and Linde*, 2002]. Colocating a seismometer, strain meter, and tiltmeter in a hole bored 100–200 m into solid rock will generally produce excellent results. With more limited resources, good results can usually be obtained with tiltmeters installed in smaller-diameter holes bored to 50–100 m depth, and in some cases, very useful data have been obtained from shallower holes or surface installations.

[39] At Unzen Volcano, Japan, a short-base, bubble-type tiltmeter was installed in a cave ~680 m west of the summit crater about a month before a dacite dome began to grow there in May 1991 [*Nakada et al*., 1999a]. For several days prior to the start of lava extrusion, the instrument recorded a changing pattern of tilt that *Yamashina and Shimizu* [1999] interpreted as follows: (1) On 11–13 May, rapid east up tilt indicated the ascent of a magma column from ~300 m to ~160 m depth beneath the vent; (2) on 14 May the rate of east up tilt decreased rapidly, suggesting that the column's ascent was interrupted; (3) on 15–16 May, rapid, south up tilt of nearly 600 μrad was caused by radial intrusion of a dike trending N80°W; and (4) on 17–19 May, southeast up tilt indicated renewed ascent of the magma column from ~160 m to the surface and continued dike intrusion. The presence of a new lava dome on the crater floor was confirmed on 20 May. Demagnetization of country rock and a swarm of high-frequency earthquakes beneath the crater also preceded emergence of the dome. These results illustrate beautifully the clarity with which magmatic processes can be inferred from high-quality monitoring data.

[40] The ongoing eruption of Soufriere Hills Volcano, Montserrat, which began in 1995 [*Robertson et al*., 2000], provides a remarkable example of the utility of tiltmeters for monitoring cyclic eruptive activity. Three tiltmeters deployed soon after the onset of the eruption at distances >1.5 km from the vent recorded no clear evidence of deformation, presumably because magma had already reached the surface. Conditions closer to the vent were hazardous and otherwise unsuitable for borehole installations, but three bubble-type biaxial tiltmeters were installed in buildings within a few hundred meters of the vent in 1996 and 1997. During dome growth they revealed repetitive 6- to 14-hour inflation cycles caused by magma pressurization a few hundred meters beneath the base of the dome. The tilt cycles correlated with seismicity, explosions, and pyroclastic flow activity and were used to forecast times of increased volcanic hazard [*Voight et al*., 1998]. *Voight et al*. [1999] proposed that the cycles reflected unsteady conduit flow of volatile-charged magma resulting from gas exsolution, rheological stiffening, and pressurization and that magma ascent rates, degassing, and microlite crystallization kinetics controlled the repeat timescale. *Denlinger and Hoblitt* [1999] noted that similar behavior is sometimes observed during high-pressure extrusion of industrial polymer melts, and they used that phenomenon as a guide to construct a simple dynamic model for oscillatory eruptive behavior.

[41] If adequate resources are available, a much better signal-to-noise ratio can be achieved with long-base tiltmeters. For example, a biaxial long-base tiltmeter has successfully tracked deformation at Long Valley caldera for more than a decade [*Behr et al*., 1992]. It uses two orthogonal tubes, 423 m and 449 m long, which are half filled with water and buried at a mean depth of 1.5 m. The water level is measured at the ends of the tubes by laser interferometer transducers. Each transducer has a water height resolution of ~0.25 μm, which corresponds to a tilt resolution of 0.6 nanorad. The ends of the tiltmeter are referenced to points 20 m deep by three borehole extensometers with displacement resolution of $\sim 5 \times 10^{-8}$ m. After correction for atmospheric pressure variation, thermal expansion, and surface displacements the instrument shows long-term stability of ~0.1 μrad per year.

[42] There are many examples of volcanic activity being effectively monitored with tiltmeters in Japan, including a notable long-base tiltmeter installation at Sakurajima Volcano. A site located 2.8 km northwest of the summit crater was chosen on the basis of modeling results using leveling data, which indicated a pressure source 3–5 km beneath the crater (for a Mogi source, maximum tilt occurs at ~1/2 the source depth). To isolate the tiltmeter from near-surface effects, a tunnel was constructed in the Harutayama lava dome specifically for this purpose. A biaxial, 28-m water tube tiltmeter and three-component extensometer were installed in the tunnel in 1985. Inflationary radial tilt in the range from 0.01 to 0.2 μrad was consistently observed for periods of 10 min to 7 hours prior to explosions in the summit crater; on that basis, automated warnings were issued for impending eruptions [*Kamo and Ishihara*, 1989].

[43] On the basis of the model results shown in Figure 4, at least 12 tiltmeters are required to reliably distinguish among possible sources: one each in the near, intermediate, and far field in each of four quadrants. Of course, the meaning of near and far field depends on the source depth, which is generally unknown. For typical volcanic sources in the depth range from 3 to 10 km a good arrangement of tiltmeters might be six instruments within 5 km of the summit, three at distances of 5–10 km, and three at 10–20 km. High-precision long-base tiltme-

ters are a better choice for more distant installations, where the predicted tilts are much smaller than at proximal sites.

[44] In summary, a comprehensive volcano-monitoring program might include on the order of 20 CGPS stations, 5 borehole strain meters, and 12 tiltmeters concentrated within 10 km of the volcano but extending out to at least 20 km. The optimal number of sensors is, of course, debatable. Some might argue for proportionally more strain meters or tiltmeters relative to CGPS stations or for more or fewer instruments based on practicality or other concerns. The details are less important than the first-order conclusion: Any realistic monitoring program designed to distinguish among plausible subvolcanic sources must include a greater number, and greater variety, of continuous sensors than have ever been deployed in the past, with few exceptions.

3.5. Satellite Radar Interferometry

[45] The foregoing discussion dealt mainly with continuous sensors, which provide the high temporal resolution necessary to capture rapidly varying deformation events. However, high spatial resolution is equally important, and for that reason, repeated large-aperture surveys also fit into a comprehensive geodetic monitoring strategy. Wherever practical, this should include routine surveillance by synthetic aperture radar (SAR) interferometry and repeated campaign-style GPS surveys. At shield volcanoes and large silicic calderas, repeated first-order leveling surveys have also been used to good advantage [*Dzurisin*, 1992].

[46] The Westdahl and Peulik interferograms suggest that global InSAR surveillance of volcanoes would be very useful. Unfortunately, this is not yet feasible for at least two reasons. First, as of June 2002 only five InSAR-capable satellites had been launched (JERS-1, ERS-1, ERS-2, RadarSat, and Envisat), and three of those were either nonoperational or no longer fully operational. Additional missions are planned or are under consideration by Japan and the United States, but the number of useful radar images of volcanoes is likely to be limited for at least the next few years. A second limiting factor is that many volcanoes are covered by ice or thick vegetation that renders C band InSAR ineffective [*Massonnet and Feigl*, 1998]. The ice problem can be partly avoided by using only images acquired during summer, but even then, the summit areas of many volcanoes are essentially inaccessible to C band InSAR. Longer-wavelength L band radars penetrate vegetation better than C band systems (albeit with somewhat lower sensitivity to ground deformation), which is a distinct advantage for most volcano applications. The proposed Japanese and U.S. SAR missions both use L band radar systems.

[47] A less serious problem with InSAR that, nonetheless, requires attention is that caused by atmospheric delay anomalies. Lateral variations in ionospheric electron density or tropospheric water vapor concentration affect the propagation of radar waves and thus can produce up to several fringes in interferograms, fringes that could mistakenly be attributed to ground deformation [*Zebker et al.*, 1997; *Massonnet and Feigl*, 1998; *Lu et al.*, 2000c; *Beauducel et al.*, 2000]. Fortunately, the recognition of delay anomalies is straightforward in most cases if several independent interferograms are available. "Independent" means that interferograms do not share a common radar image. For example, interferogram 1 constructed from images A and B and interferogram 2 constructed from images C and D are independent. However, interferogram 1 and interferogram 3 constructed from images B and E are not independent, because they both use image B. If B includes an atmospheric delay anomaly, it would produce a similar fringe pattern in interferograms 1 and 3 but not in interferogram 2. In contrast, any fringes caused by deformation would be present in all three interferograms if they spanned the time period of the deformation. Thus comparison of independent interferograms that span similar time periods can usually distinguish between the effects of atmospheric delay anomalies and ground deformation.

[48] This strategy can fail, however, if delay anomalies are persistent or recurring, as might be the case near volcanoes with large topographic relief. Tall volcanoes can influence local weather patterns and set up quasi-steady patterns of water vapor concentration both horizontally and vertically (e.g., windward clouds and leeward clear skies or summit cap clouds and sunny flanks). Such quasi-steady tropospheric patterns might be especially troublesome at large volcanoes such as Mount Etna, Italy [*Beauducel et al.*, 2000], and Mauna Loa, Hawaii.

[49] Near-term problems aside, InSAR has established itself as an essential technique for monitoring volcano deformation, especially in remote areas where other forms of geodetic monitoring are difficult or impractical. In such places the lack of an adequate digital elevation model (DEM) is sometimes a problem for InSAR, but this should be alleviated by the planned release of a global DEM with at least 3-arc-sec resolution (~90 m) from NASA's Shuttle Radar Topography Mission. Even at accessible volcanoes that are well monitored by other techniques, InSAR offers an unparalleled degree of spatial coverage and completeness (decameter-scale spatial resolution over $\sim 10^4$ km^2 per image). No other technique is capable of imaging the deformation field as thoroughly, either in the far field where repeated surveys are typically sparse or in the near field where deformation can be very complex. Although the specifics will be dictated by the designs of future InSAR missions, an ideal volcano surveillance program would include L band and preferably also C band imaging at monthly intervals during quiescence and daily intervals during periods of unrest.

3.6. Repeated GPS Surveys

[50] Repeated GPS surveys are another useful tool for measuring volcano deformation, although with considerably less spatial and temporal resolution than InSAR

and continuous sensors, respectively. On the plus side, GPS surveys can cover a broad area relatively quickly, do not require long-term maintenance of equipment in the field, and provide millimeter- to centimeter-scale resolution of surface displacements in three dimensions. InSAR provides much better spatial coverage but with less sensitivity to small surface displacements (i.e., 10–20 mm in the range direction only for C band InSAR, compared to 2–3 mm horizontal and 10–15 mm vertical for GPS surveys). A combination of relatively continuous sensors for temporal completeness and repeated (monthly to yearly) InSAR and GPS surveys for spatial completeness comes reasonably close to the goal of monitoring deformation "everywhere, all the time."

3.7. Microgravity Measurements

[51] Even if the surface deformation field is well characterized in space and time by a combination of the techniques discussed in sections 3.6–3.6, the physical mechanism(s) responsible for deformation can still be ambiguous. For example, episodes of crustal uplift and subsidence at the Yellowstone caldera, Wyoming, have been documented by repeated leveling and GPS surveys and by an InSAR study. Nonetheless, the geodetic data do not distinguish between two source models, with very different implications for the current state of the Yellowstone magmatic system. Deformation might be caused by episodic intrusions of magma beneath the caldera or by pressurization/depressurization cycles that occur in the deep hydrothermal system while the underlying magmatic system cools [*Smith et al.*, 1997; *Wicks et al.*, 1998; *Dzurisin et al.*, 1999]. The shape of the surface deformation field alone cannot distinguish between these alternatives, because both sources are relatively deep (5–10 km) and centered beneath the caldera. However, the two models predict different linear relationships between height change and gravity change, so concurrent microgravity and leveling or GPS surveys can be very useful for distinguishing among alternative models at Yellowstone and other restless volcanoes.

[52] Gravity measurements can be made either continuously or episodically. It is very important to measure any changes in surface height or groundwater levels concurrently, so their effects can be removed from the gravity observations. Any remaining Bouguer gravity change can be attributed to a change in subsurface mass or density. In many cases the most likely cause is magma movement, either toward the surface or laterally along a rift zone or fracture. At Long Valley, for example, repeated leveling and microgravity surveys combined with water level data from several wells provide conclusive evidence for an increase in mass beneath the caldera from 1983 to 1998 [*Battaglia et al.*, 1999], a period that also included sporadic earthquake swarms, uplift of the resurgent dome, and increased CO_2 emission [*Hill et al.*, 2002]. The occurrence of uplift and extension was known from several types of measurements, and inflation of a subcaldera magma body was the favored explanation. However, it was unclear whether inflation was caused by magma intrusion or pressurization by magmatic volatiles [*Tait et al.*, 1989] until the gravity study produced compelling evidence for a mass increase.

[53] An effective strategy for monitoring changes in gravity, groundwater level, and surface height is to combine repeated surveys of an extensive network of stations with continuous measurements at a few key sites. Wherever possible, such a strategy should be an integral part of a comprehensive volcano-monitoring program.

4. SOME EARLY STEPS TOWARD COMPREHENSIVE GEODETIC MONITORING

4.1. Mount St. Helens GPS Network

[54] Guided by the precepts outlined in section 3, the USGS Cascades Volcano Observatory established a 40-station GPS network at Mount St. Helens during summer 2000 (Figure 5). Although the network is concentrated within 10 km of the summit, it extends >30 km in all directions and covers a total area of >7400 km^2. Four CGPS stations are located within the network to capture any short-term deformation and to help with atmospheric corrections. These include one dual-frequency P code station at the U.S. Forest Service's Johnston Ridge Observatory (8 km north of the central crater) and three single-frequency stations within 5 km of the crater: one on the 1980–1986 lava dome and one each to the east and west. The 2000 survey established a baseline for future surveys, which are planned at least every few years. Annual surveys are preferable but not currently practical owing to limited resources.

[55] The Mount St. Helens GPS network is considerably larger than most geodetic networks at volcanoes, and some might argue that benchmarks more than 10 km from the summit are extraneous for monitoring volcanic activity. That view is based on decades of experience and has considerable merit from a short-term monitoring perspective. Most eruptions are preceded by days to months of intense, shallow-seated unrest, mainly earthquakes and ground deformation concentrated within a few kilometers of the vent. At such times, short-term eruption prediction is an immediate concern and monitoring far-field deformation (i.e., beyond ~10 km) justifiably receives lower priority in most cases. Conversely, during volcanic quiescence or even during a crisis if adequate resources are available, broad-scale geodetic surveys make good scientific sense. They address a different suite of questions than most other forms of monitoring, which are directed toward understanding the immediate cause and likely outcome of unrest. For example, broad-scale geodetic surveys can address such general questions as the following.

1. What interactions occur among magmatic systems, regional strain, and large earthquakes? Does basalt influx into the crust beneath volcanoes occur in response to large regional earthquakes?

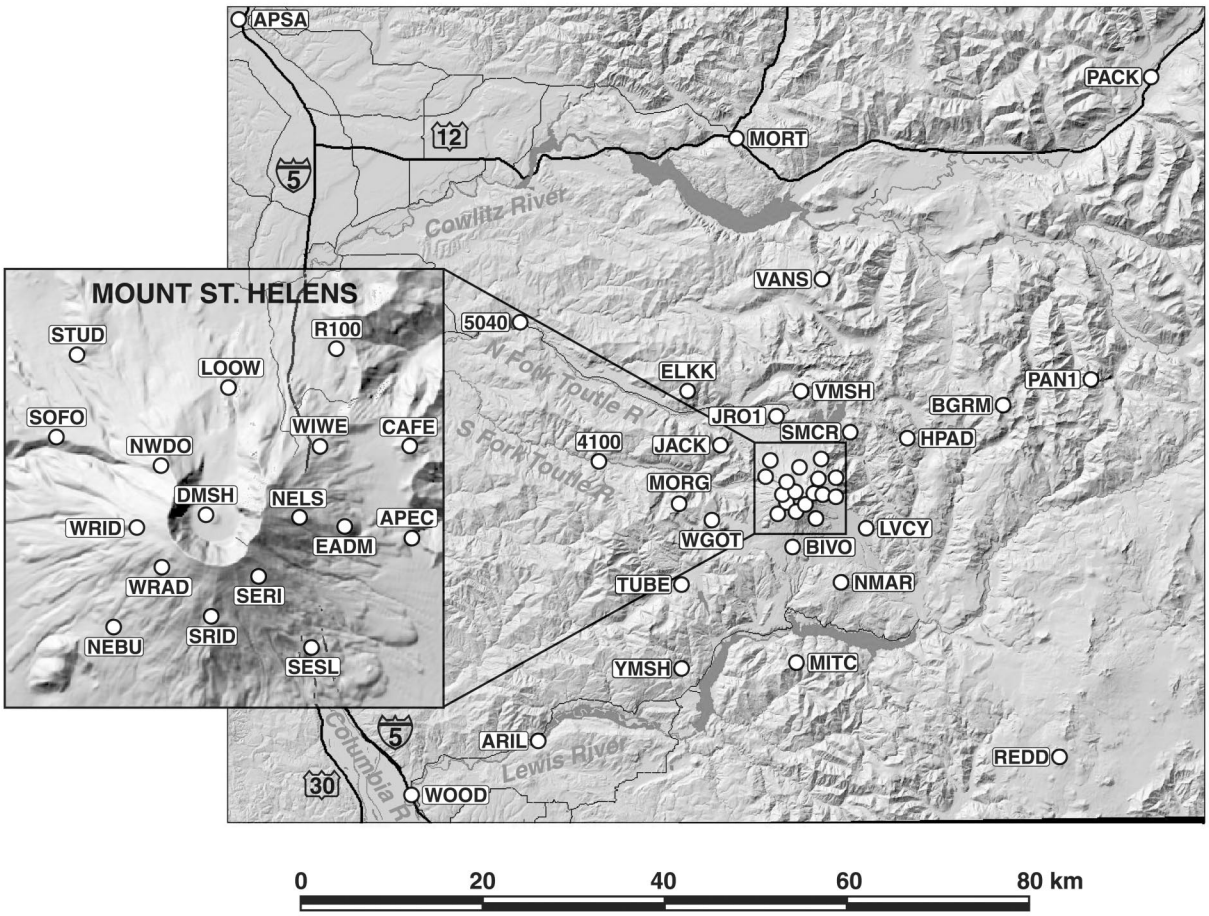

Figure 5. Mount St. Helens large-aperture GPS network, including 40 benchmarks installed and observed during summer 2000, superimposed on a shaded relief version of a USGS digital elevation model. The network is designed to capture both near-field and far-field deformation from magmatic sources near or above the brittle-ductile transition and also tectonic deformation within the St. Helens Seismic Zone. Graphic is by S. Schilling and M. Howell (personal communication, 2001). See color version of this figure at back of this issue.

2. Where, when, and how does magma accumulate beneath volcanoes? Does magma recharge occur gradually or episodically throughout the eruption cycle? Can the onset of shallow-seated unrest be anticipated by monitoring the amount of recharge?

3. Does far-field deformation hold clues to the style and magnitude of eruptions? Can we discriminate between intrusive events that stall and those that culminate in eruptions?

[56] Recent examples of volcanic unrest or eruptions that included far-field seismicity or ground deformation include Unzen, Japan, prior to its 1990–1995 eruption [*Nakada et al*., 1999a], Karymsky and Akademia Nauk Volcanoes, Russia, which erupted simultaneously ~14 hours after the main shock (M_s 6.6) of a remarkably strong foreshock–main shock–aftershock sequence in January 1996 [*Zobin and Levina*, 1998], and the Yellowstone and Long Valley calderas, United States, which have been restless for decades and exhibit clear signs of magmatic-tectonic interaction [*Dzurisin et al*., 1999; *Smith et al*., 1997, 1999; *Hill et al*., 1990, 1993, 1995].

[57] Of course, a broad-scale GPS network is only one component of a balanced volcano geodesy program. At Mount St. Helens, there is a continuing need for additional CGPS stations and continuously recording strain meters and tiltmeters, the latter preferably installed in boreholes where near-surface noise sources would be greatly attenuated.

[58] A striking demonstration of the importance of extending geodetic networks at volcanoes well into what would normally be considered the far field for volcanic deformation was recently provided by an InSAR study of the Three Sisters volcanic center, Oregon. Interferograms reveal a broad domical uplift centered ~5 km west of South Sister Volcano, which occurred between August 1996 and October 2000 [*Wicks et al*., 2002] (Figure 6). An elastic point source model indicates a volume increase by 0.023 ± 0.003 km^3 located 6.5 ± 0.4 km beneath the surface, presumably a magmatic intrusion. The deformation field extends across EDM and tilt-leveling networks that were established in 1985 and remeasured in 1986 in anticipation of future activity at

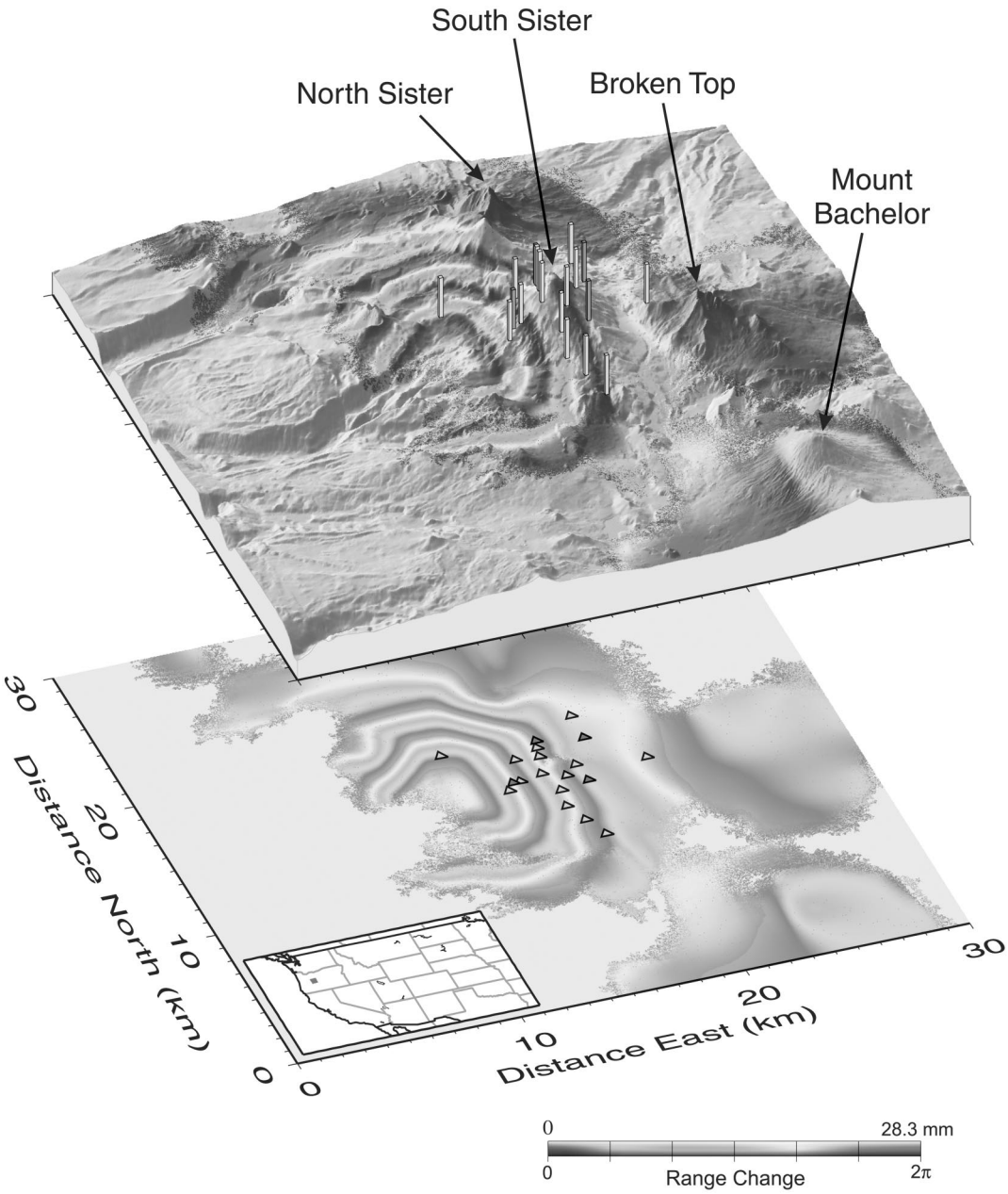

Figure 6. Interferogram of the Three Sisters area, central Oregon Cascade Range, for the period 20 August 1996 to 10 October 2000 [*Wicks et al*., 2002] showing the locations of electronic distance measurement (EDM) benchmarks (cyan bars and triangles) and tilt-leveling benchmark arrays (red bars and triangles) at South Sister. Each interferometric fringe represented by a color band from violet to red represents 2.83 cm of range change from satellite to ground. Approximately four fringes centered 5 km west of South Sister volcano correspond to ~11 cm of surface movement toward the satellite (mostly uplift). The EDM and tilt-leveling networks were established in 1985 and remeasured in 1986 as a baseline to monitor deformation at South Sister [*Iwatsubo et al*., 1988]. They do not extend across the entire deformation field revealed in the interferogram, which illustrates the importance of extending deformation networks well beyond the volcanic edifice to increase the likelihood of capturing far-field or eccentric deformation. See color version of this figure at back of this issue.

South Sister [*Yamashita and Doukas*, 1987; *Iwatsubo et al*., 1988]. Reobservation of the networks during summer 2001 (the former by GPS) yielded useful information about the uplift, but much broader networks are needed to span the entire deformation field.

[59] Both generalized modeling results and specific ground deformation episodes such as those near Three Sisters and Mount Peulik suggest that geodetic networks should extend at least 20 km in all directions from potential vent areas. This is especially true in volcanic areas prone to spatially distributed vents such as the central Oregon Cascades and the Lassen volcanic center and the Long Valley-Inyo-Mono Craters region (northern and east central California, respectively).

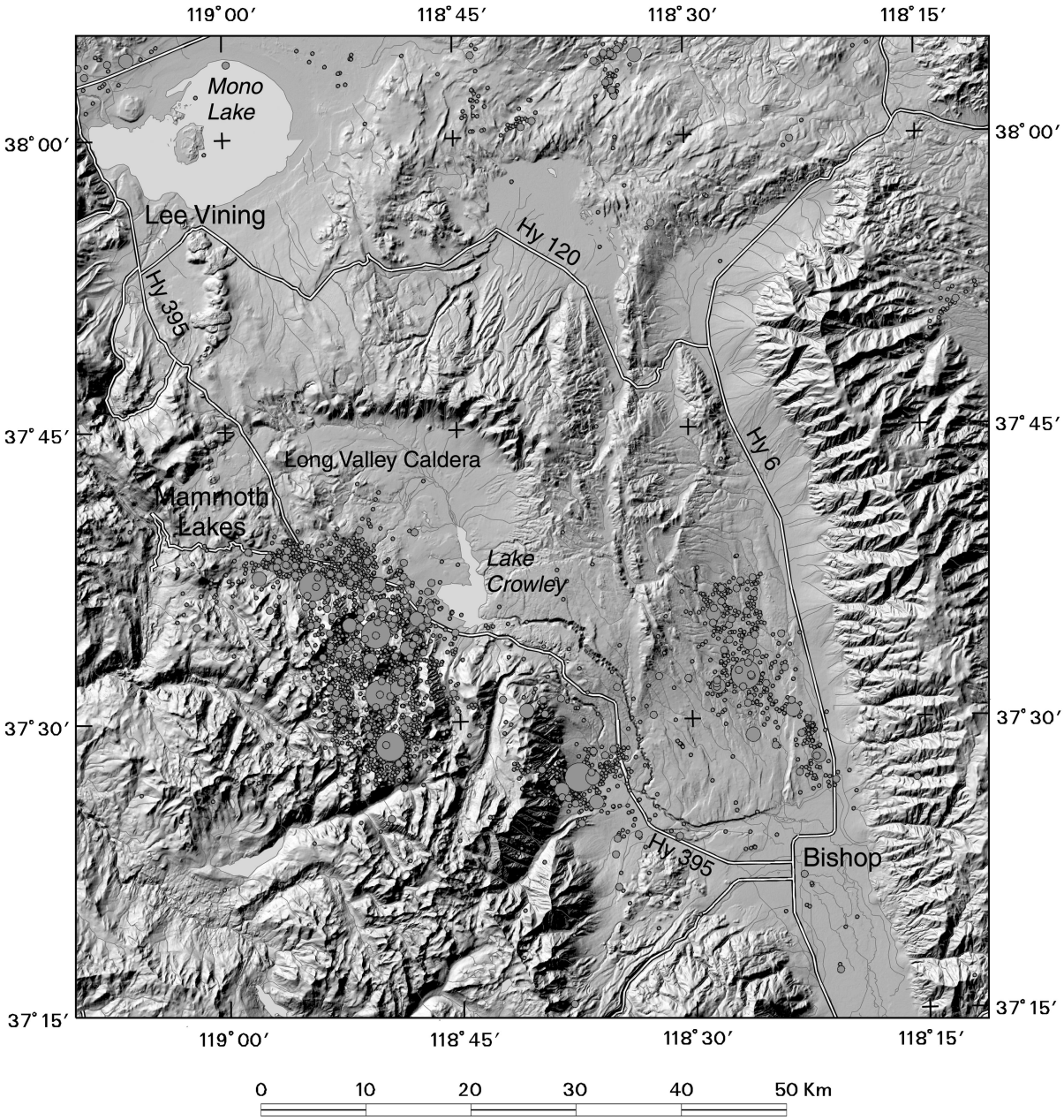

Figure 7. Shaded relief map of the Long Valley region showing epicenters of earthquakes larger than magnitude 3 (circles) for the period 1978–1999 [from *Hill et al*., 2002]. Largest circles represent events with $5.5 < M < 6.5$. A prolonged episode of unrest began with the M 5.7 Wheeler Crest earthquake on 4 October 1978, midway between the towns of Bishop and Mammoth Lakes. Thereafter sporadic earthquake activity migrated toward the caldera until on 25–27 May 1980 four M 6 events struck beneath the caldera's south moat and adjacent Sierra Nevada block. Subsequent activity has been concentrated in the same area and also beneath Mammoth Mountain, a young cumulovolcano located along the caldera's southwest rim near Mammoth Lakes. The M 6.1 Round Valley earthquake occurred on 23 November 1984, ~10 km NNW of Bishop. Since 1980, ground deformation has been centered at the resurgent dome in the west central part of the caldera, an area that produces very few earthquakes. See color version of this figure at back of this issue.

4.2. Intensive Geodetic Monitoring of Long Valley Caldera

[60] The Long Valley caldera has been restless for more than 2 decades and is among the most intensively studied magmatic systems in the world [*Hill*, 1999; *Hill et al*., 1995] (Figures 7 and 8). As such, it serves as an excellent example of what can be accomplished through a comprehensive, long-term approach to volcano monitoring. In mid 2002 the Long Valley seismic network included ~18 stations within and immediately adjacent to the caldera and an additional 17 stations within 50 km of the caldera [*Hill*, 1984; *Hill et al*., 1990, 2002] (Figure

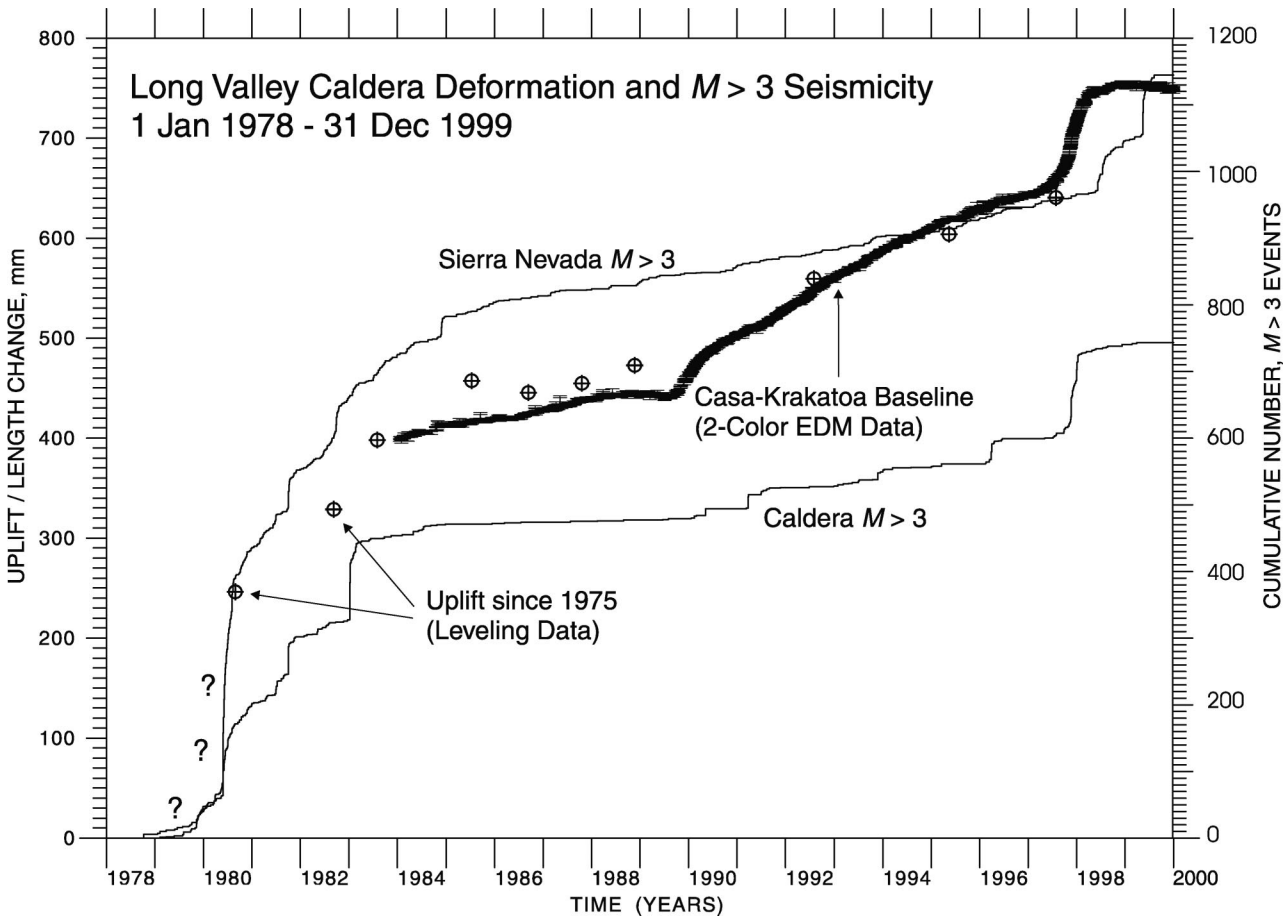

Figure 8. Time series plot of seismicity and ground deformation near Long Valley caldera for the period 1978–1999 [from *Hill et al.*, 2002]. Plot includes (1) cumulative numbers of $M > 3$ earthquakes beneath the caldera and adjacent Sierra Nevada block, (2) uplift of the resurgent dome near Casa Diablo from repeated leveling surveys, and (3) extension of a baseline across the resurgent dome from repeated two-color EDM measurements (see Figure 10a for location of EDM stations Casa and Krakatoa). Rapid uplift and extension within the caldera during 1980–1983 and 1997–1998 was accompanied by intense seismicity beneath the caldera's south moat and the adjacent Sierra Nevada block, presumably as a result of magmatic inflation beneath the resurgent dome [*Langbein et al.*, 1995]. In 1989 an increase in the caldera extension rate preceded an earthquake swarm beneath Mammoth Mountain that marked an intrusion of basaltic magma to within a few kilometers of the surface [*Hill et al.*, 1990]. Another episode of rapid caldera inflation and seismicity began in late 1997; activity has since declined to background levels.

9). The geodetic monitoring effort included (1) a two-color EDM network that spans the resurgent dome, south caldera moat, and Mono-Inyo volcanic chain, (2) 10 continuous GPS stations, (3) four Sacks-Evertson borehole strain meters, (4) seven borehole tiltmeters and one L-shaped long-base (0.5 km) Michelson interferometer tiltmeter, (5) 10 differential magnetic field stations, (6) two magnetotelluric arrays, (7) a first-order leveling network comprising ~200 km of leveling lines, and (8) a dense GPS network that spans the caldera and Mono-Inyo volcanic chain (Figures 10–13). GPS and leveling surveys are conducted every few years or annually during periods of heightened activity. Regional deformation is also being studied with InSAR [*Simons et al.*, 1996]. Other types of monitoring include continuous and survey-mode CO_2 emissions (ground-based and airborne), water well levels, stream discharge, and fumarole conditions.

[61] More than 2 decades of intensive, interdisciplinary research at Long Valley has revealed much about the structure and dynamics of the Long Valley and Mono-Inyo magmatic systems, including new insights into volcano-tectonic interactions, temporal relationships among magmatic inflation, ground deformation, seismicity, surface outgassing, and the mechanism of triggered seismicity at large magmatic systems. How these factors relate to the next eruption in the region is, of course, not yet known. For our purposes, the Long Valley experience serves as a valuable case study of what can (and cannot) be learned from a comprehensive volcano geodesy program, provides useful guidance toward the most effective geodetic tools in various situa-

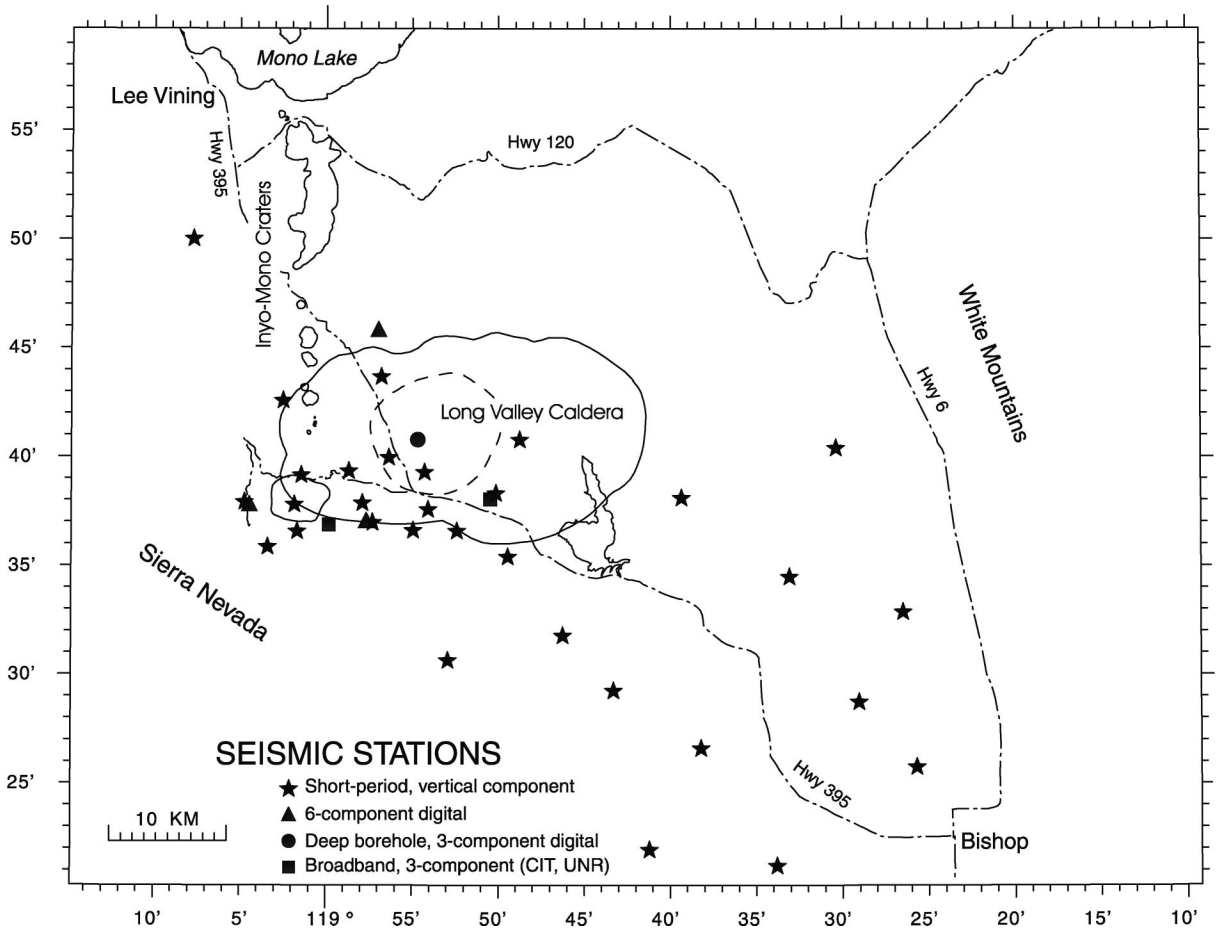

Figure 9. The Long Valley seismic network, which includes ~18 stations within and immediately adjacent to the caldera and an additional 17 stations within 50 km of the caldera [*Hill et al.*, 2002].

tions, and points the way toward next-generation volcano-monitoring programs.

[62] Perhaps the most significant outcome of the Long Valley research effort to date is improved understanding of the magma storage and transport system beneath Long Valley caldera and adjacent Mammoth Mountain. Several sources that have been active during the current episode of unrest have been postulated primarily from modeling of ground deformation patterns. These include [*Langbein et al.*, 1995] (1) an ellipsoidal source 5.5 km beneath the resurgent dome that accounts for >90% of the observed deformation inside the caldera, (2) an ellipsoidal source or pipe 10–20 km beneath a persistent locus of earthquake activity in the south moat, (3) a northwest trending, northeast dipping dike beneath the southwest part of the caldera, (4) a dike from 2 to 12 km beneath Mammoth Mountain, and (5) a dike beneath the Mono-Inyo Craters volcanic chain. This combination of sources, like most geodetic modeling results, is nonunique. Nonetheless, it provides a useful framework for interpreting future events in the region.

[63] Another important result from Long Valley, especially from a geodetic perspective, is the relative timing among various manifestations of unrest, primarily seismicity, ground deformation, and volcanic gas emissions. The current episode of unrest began at about the time of the M 5.4 Wheeler Crest earthquake, which struck midway between the towns of Bishop and Mammoth Lakes (Figure 7) on 4 October 1978. Thereafter clusters of small to moderate ($M > 4$) earthquakes generally migrated northwestward toward the caldera until on 25–27 May 1980 four M 6 earthquakes and an intense swarm of smaller events shook the region. Frequent earthquake swarms, notably in January 1983 (south moat) [*Savage and Cockerham*, 1984], 1989–1990 (Mammoth Mountain) [*Hill et al.*, 1990], and late 1997 (south moat), have been accompanied by ~80 cm of net uplift of the resurgent dome, changes in the shallow hydrothermal system, and increased emission of magmatic CO_2 in the vicinity of Mammoth Mountain [*Hill*, 1996].

[64] Leveling and EDM surveys made soon after the May 1980 seismic crisis revealed that the resurgent dome had risen ~25 cm and the caldera had extended substantially since the previous surveys [*Savage and Clark*, 1982], but the relative timing of the seismicity and deformation remains unknown. Similarly, leveling surveys made during the summers of 1982 and 1983 showed that an intense swarm of earthquakes beneath the south moat in January 1983 was associated with ~7 cm of additional

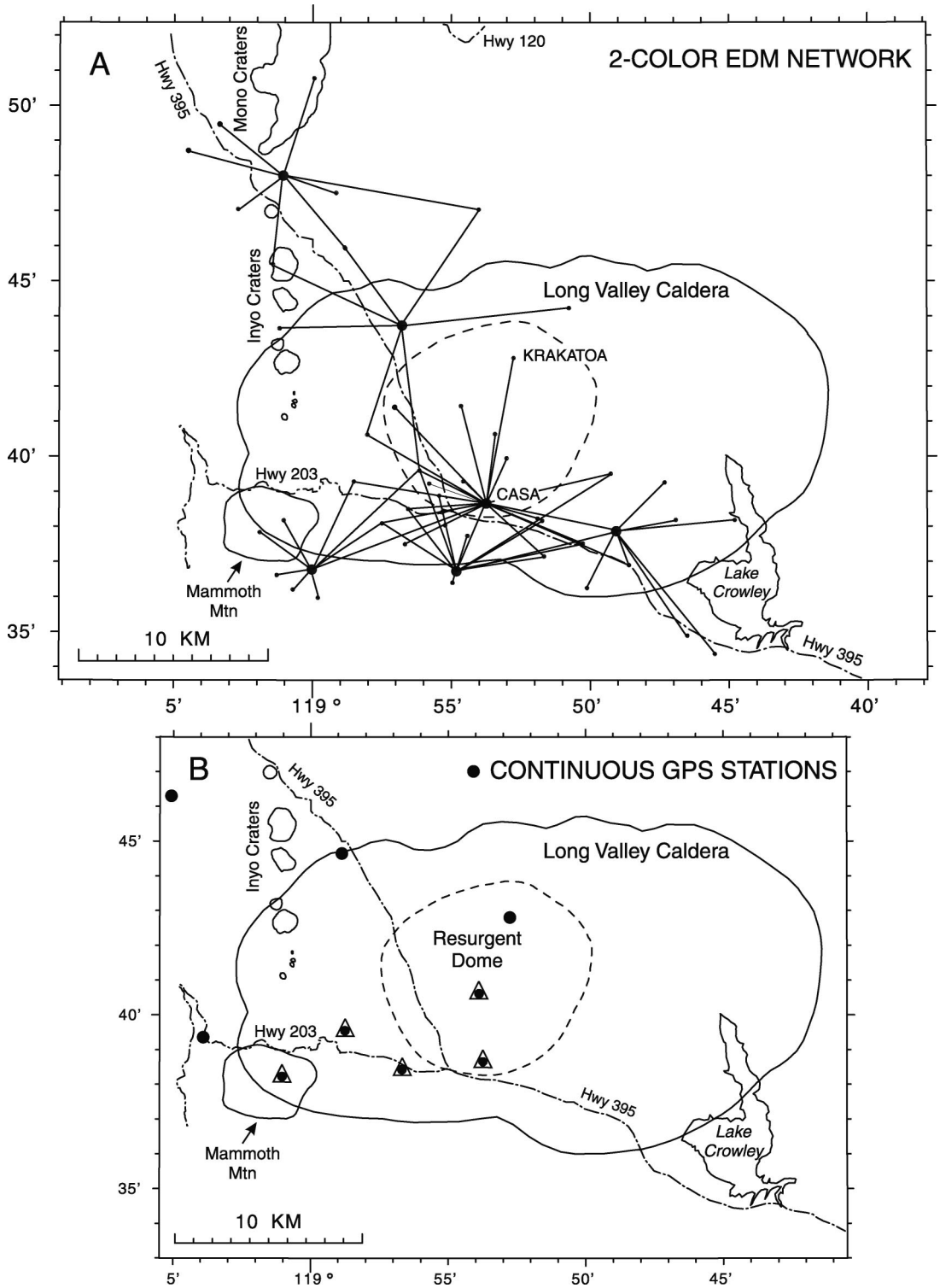

Figure 10. (a) Configuration of the two-color EDM network and (b) CGPS stations near Long Valley caldera [*Hill et al*., 2002]. Several EDM lines from Casa are measured every few days; the rest of the network is measured monthly or yearly. In Figure 10b, circles with triangles represent CGPS stations with real-time data processing [*Endo and Iwatsubo*, 2000].

uplift of the dome [*Savage and Cockerham*, 1984], but it is not known whether some of the uplift preceded, accompanied, or followed the swarm.

[65] The timing issue has been clearly resolved in at least one instance by frequent two-color EDM measurements, which demonstrate the importance of ground deformation as an early indicator of magmatic unrest. The EDM data show that extensional strain rates in the south moat gradually decreased from as high as 5 ppm/yr several months after the January 1983 earthquake

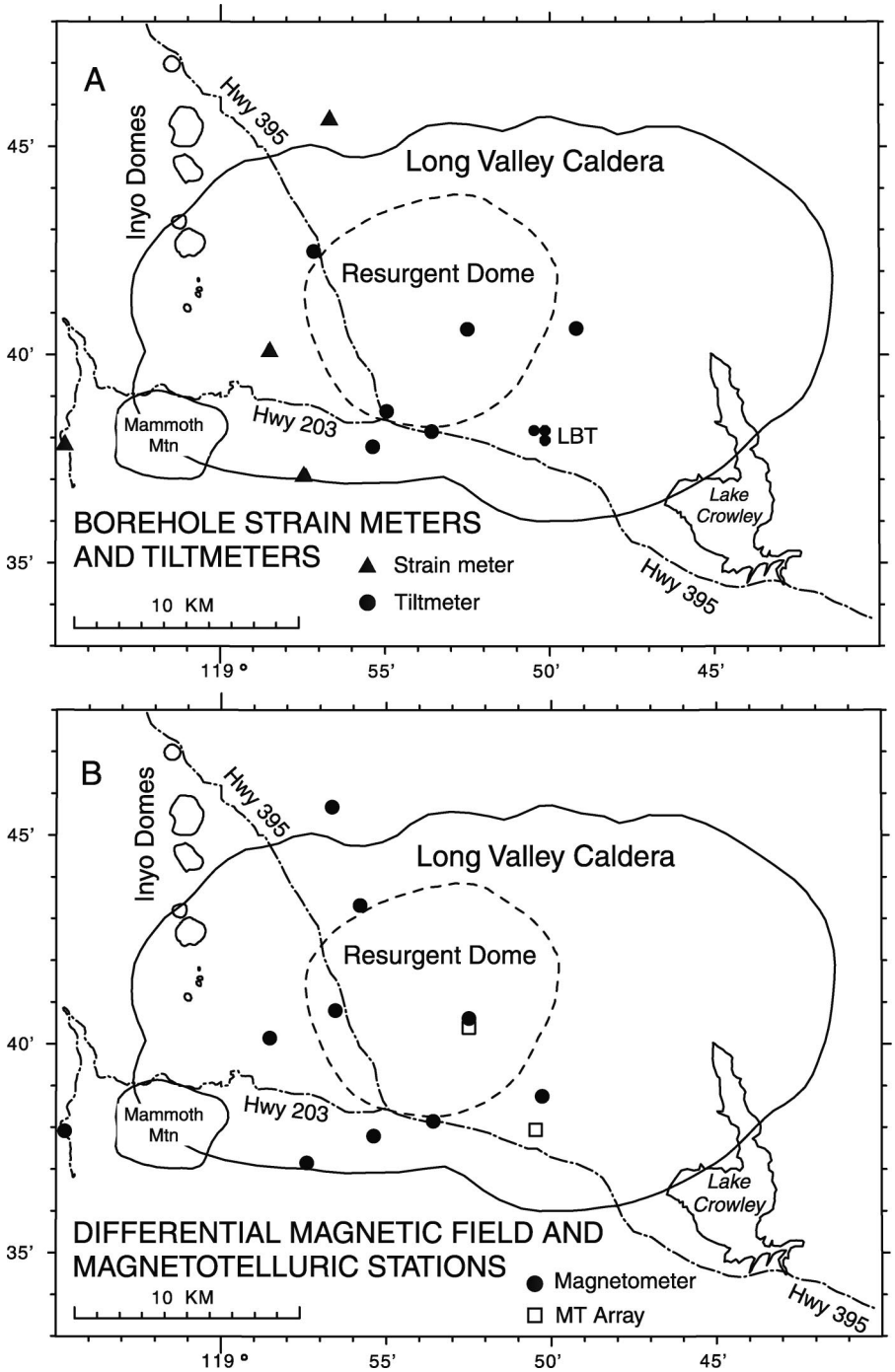

Figure 11. (a) Borehole strain meters and tiltmeters and (b) differential magnetometers and magnetotelluric stations near Long Valley caldera [*Hill et al.*, 2002]. In Figure 11a, LBT is an L-shaped long-base (~0.5 km north-south and east-west) Michelson interferometer tiltmeter.

swarm to near zero in mid 1989 [*Langbein et al.*, 1993]. Then, starting in October 1989, a remarkable thing happened (Figure 8). Extension rates increased to as high as 9 ppm/yr over a period of a few weeks, while the level of earthquake activity beneath the south moat and elsewhere in the caldera remained low. About 2 weeks later, a subtle increase in the occurrence of small earthquakes beneath Mammoth Mountain was noted. This area had been relatively quiet since the beginning of unrest more than a decade earlier. Earthquake activity beneath the caldera also picked up several weeks later, in December 1989, and continued at an elevated level through 1991. The EDM results clearly foretold increases in earthquake activity beneath Mammoth Mountain and the caldera, but what processes were at work to cause the earthquakes?

[66] There is compelling evidence that seismicity beneath Mammoth Mountain during 1989–1990 was

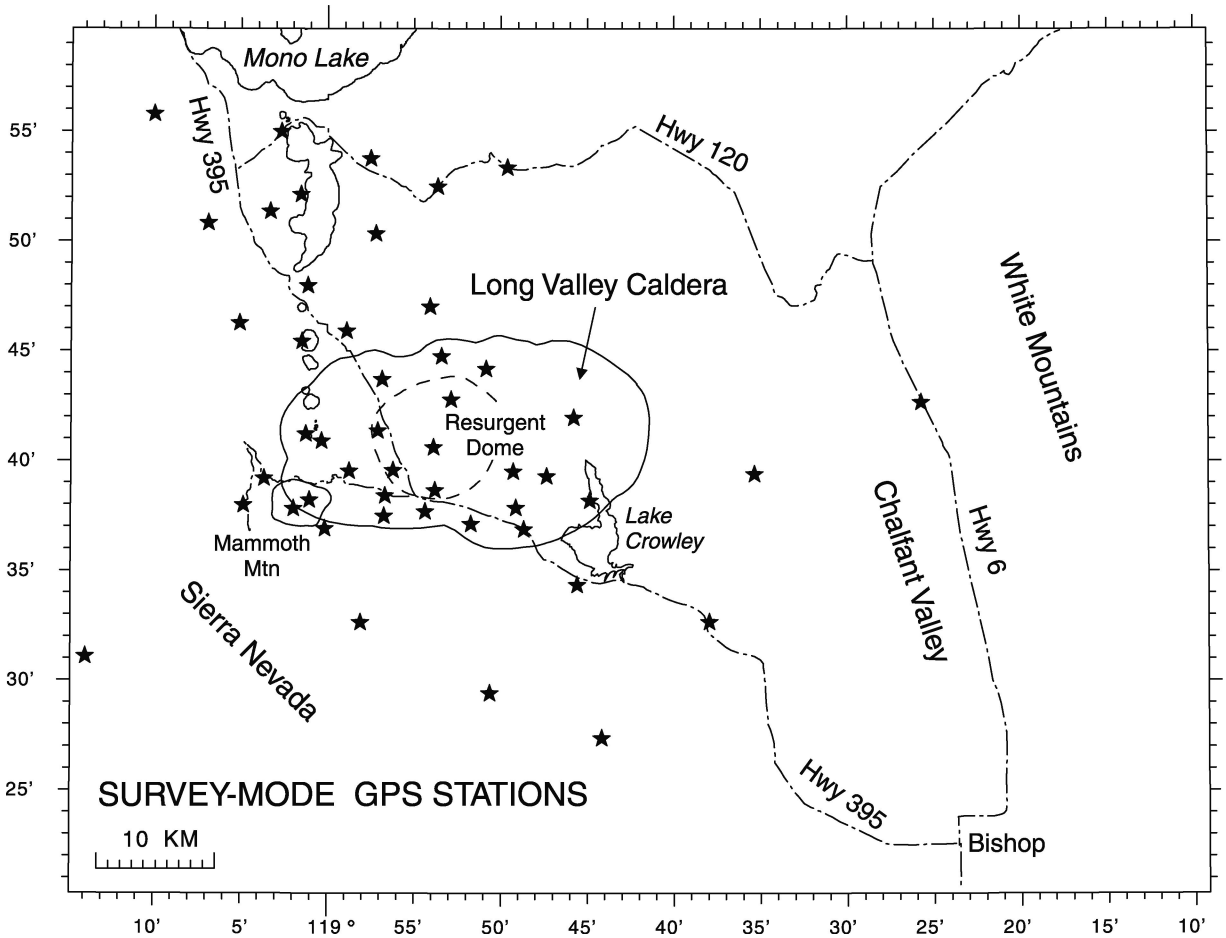

Figure 12. Regional survey-mode GPS network near Long Valley caldera [*Hill et al.*, 2002], which is measured every few years or more often in response to increased activity.

caused by intrusion of magma into the upper crust beneath the volcano. Renewed inflation beneath the caldera starting several weeks later was probably caused by a separate intrusion into a magma reservoir located ~6 km beneath the resurgent dome. Evidence for an intrusion beneath Mammoth Mountain includes [*Hill*, 1996] the following: (1) a dike-like distribution of hypocenters at depths of 6–9 km with a NNE strike essentially perpendicular to the *T* axes of the earthquake focal mechanisms [*Hill et al.*, 1990]; (2) deformation in the vicinity of Mammoth Mountain consistent with a NNE striking dike extending to within 2 km of the surface [*Langbein et al.*, 1993]; (3) frequent spasmodic bursts of seismicity suggesting rapid-fire brittle failure driven by transient surges in local fluid pressure [*Hill et al.*, 1990]; (4) an increase in $^3He/^4He$ ratios from fumaroles on Mammoth Mountain detected in late 1989 [*Sorey et al.*, 1993]; (5) a persistent sequence of long-period (LP) volcanic earthquakes beneath the southeast flank of Mammoth Mountain at depths between 10 km and 30 km; and (6) accelerated outgassing of CO_2, almost surely of magmatic origin, around the flanks of Mammoth Mountain first noticed when trees began dying in the area during 1990 [*Farrar et al.*, 1995; *McGee and Gerlach*, 1998].

[67] A third significant finding at Long Valley is the degree to which the magmatic system is sensitive to distant large earthquakes. Triggered responses to distant earthquakes at Long Valley and elsewhere challenge conventional wisdom and raise some intriguing possibilities concerning the link between regional tectonism and magmatism. The 1992 M_w 7.3 Landers, California, earthquake [*Hill et al.*, 1995] and the 1999 M_w 7.1 Hector Mine, California, earthquake [*Freed and Lin*, 2001] both triggered transient strain pulses and bursts of seismicity beneath Long Valley and other widely scattered sites across the western United States. What mechanism or mechanisms account for triggered responses over such great distances? The Landers case is illustrative.

[68] The observed coseismic static dilatational strain in the vicinity of Long Valley caldera from the Landers main shock was a 0.006-μstrain (~0.003 bar) compressional step, which is about an order of magnitude smaller than daily tidal stress fluctuations and therefore is not a viable mechanism for the triggered seismicity. Peak dynamic stresses, however, were ~3 bars, plausibly large enough to trigger one or more responses:

1. *Linde et al.* [1994] suggested that the dynamic waves from Landers triggered a transient pressure increase in one or more magma bodies by advective over-

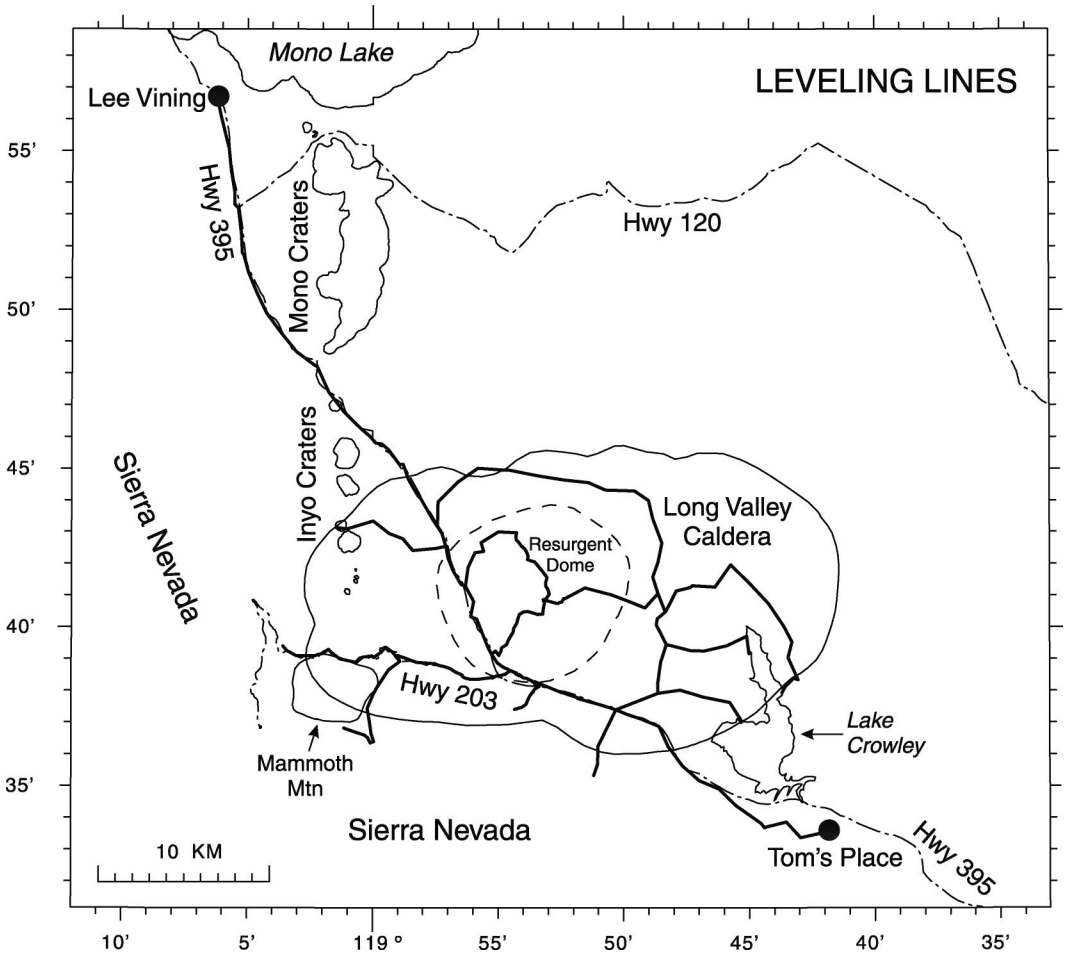

Figure 13. Long Valley first-order leveling network (bold lines) [*Hill et al.*, 2002]. The traverse along Highway 395 between Lee Vining and Tom's Place was measured 11 times from 1980 to 1997; more extensive surveys were conducted annually from 1983 to 1988 and in 1992.

pressure (i.e., bubble formation and ascent), which, in turn, triggered the observed seismicity and strain.

2. *Johnston et al.* [1995] proposed that the dynamic strains from Landers ruptured compartments of superhydrostatic fluid pressures, which are commonly encountered in volcanic and geothermal regions [*Fournier*, 1991]. They suggested that the result was an upward surge of fluids in the crust beneath the caldera by hydraulic fracturing.

3. *Anderson et al.* [1994] and *Bodin and Gomberg* [1994] hypothesized that the shear pulse from Landers initiated aseismic slip on midcrustal faults beneath the caldera, and the associated deformation induced brittle failure at shallower depths.

4. *Hill et al.* [1995] proposed that large, low-frequency strains from Landers might have fluidized a partially crystallized magma body beneath the caldera, thereby releasing some of the differential stress supported by the solid phase (crystals). Alternatively, large dynamic stresses from Landers might have induced a magmatic intrusion into the lower crust beneath the caldera. Either process occurring at a depth of ~60 km beneath the caldera satisfies all existing constraints.

[69] All four of these models explain the essential features of Long Valley's response to the Landers earthquake, but one may be more generally applicable than the others. Most of the seismicity triggered by Landers was concentrated along the margins of the Basin and Range province [*Hill et al.*, 1993], where deep zones of basaltic magma are likely drawn into the lower crust by extension [*Lachenbruch et al.*, 1976]. The relaxing magma body or dike intrusion model can thus account for triggered seismicity at many widely dispersed and diverse sites. As noted by *Hill et al.* [1995, p. 13,002], "If this model is correct, it suggests that significant influx of basaltic magma into the deep roots of crustal magmatic systems occurs episodically in response to large, regional earthquakes. This in turn offers a specific link between regional tectonism and magmatism."

[70] The picture that emerges at Long Valley is one of complex, space- and time-varying interactions among tectonic, magmatic, and hydrothermal processes that have yet to reach a conclusion. Regardless of the outcome, the value of an ambitious program of geodetic measurements for monitoring unrest at large silicic calderas has been firmly established, as it was several

decades earlier for basaltic shield volcanoes in Hawaii and arc volcanoes in Japan.

4.3. Volcano Research in Japan: Insights From Integrated Volcano-Tectonic Studies

4.3.1. Earthquake and Eruptive Activity Near the Izu Peninsula, Japan

[71] A remarkable sequence of volcano-tectonic events has occurred near the Izu Peninsula, central Japan since the *M* 6.9 Izu-Hanto-Oki earthquake in 1974. That shock was preceded by 40 years of relative quiescence and followed by the 1976 *M* 5.4 Kawazu earthquake, the 1978 *M* 7.0 Izu-Oshima-Kinkai earthquake, the 1980 *M* 6.7 Izu-Hanto-Toho-Oki earthquake, and the 1990 *M* 6.5 Izu-Oshima-Kinkai earthquake. Meanwhile, there have been more than a dozen earthquake swarms associated with magmatic intrusions, broad uplift of the eastern part of the peninsula, and two offshore eruptions. The first was a submarine eruption near Ito City, which began on 13 July 1989 [*Okada and Yamamoto*, 1991]. The second was accompanied by formation of a small collapse caldera atop Miyake Island in July–August 2000 [*Kumagai et al.*, 2001].

[72] Documentation of the eruption near Ito includes continuous tilt and seismic records from a 92-m borehole within 5 km of the eruption site, continuous records from two borehole strain meters within 20 km, daily laser distance measurements of a 10-km baseline that crosses within 1 km of the site, daily GPS monitoring of a 10-km baseline that crosses within 2 km, repeated EDM surveys of several other baselines that span the site, and repeated leveling surveys along the east coast of Izu Peninsula within 4 km of the site [*Okada and Yamamoto*, 1991]. The tiltmeter began detecting unusual tilt in late May 1989, which changed direction and accelerated on 4 July and again on 8 July, then stopped abruptly on 11 July 2 days before the eruption on 13 July. The total amount of tilt during July was more than 20 μrad [*Yamamoto et al.*, 1991]. The strain meters also detected the first anomalous activity, in this case 5×10^{-7} contractional strain, in late May 1989 and then 1×10^{-6} of additional contraction starting in early July. The latter signal stopped abruptly on 9 July with the occurrence of an *M* 5.5 earthquake, the largest in the sequence. Also, during the first week of July the laser distance baseline extended by 23 ± 1 cm [*Shimada et al.*, 1990; *Fujinawa et al.*, 1991], the nearby GPS baseline extended 14.5 ± 0.4 cm, and several ~10-km EDM baselines lengthened by 16–17 cm. Leveling surveys in June and July 1989 revealed that the central part of Ito City was uplifted >8 cm, and bathymetric surveys discovered that a knoll, 25 m high and 300 m in diameter, formed on the seafloor between 9 July and 13 July. On 13 July a phreatomagmatic eruption from the top of the knoll produced a 200-m-diameter crater [*Oshima et al.*, 1991].

[73] *Okada and Yamamoto* [1991] modeled this rich geodetic data set as two tensile faults (dikes) corresponding to magmatic intrusions in May and July 1989 and a right-lateral reverse fault representing the *M* 5.5 earthquake on 9 July. Intersection of the reverse fault and one of the dikes caused magma to intrude into soft seafloor sediments, creating a lava dome. The 13 July phreatomagmatic eruption was shallow-seated and did not produce any measurable deformation.

[74] Another notable earthquake swarm and intrusion occurred off the east coast of the Izu Peninsula in March 1997. Borehole instruments recorded tilt, volumetric strain, and water level changes starting several hours before the swarm onset. A similar pattern was observed during prior and subsequent swarms, which led *Okada et al.* [2000] to infer that intrusions at depth cause deformation but only start generating earthquake swarms when they reach the base of the seismogenic zone (i.e., the brittle-ductile transition) at ~10 km depth. The spatiotemporal evolution of the propagating dike after it reached the seismogenic zone was estimated from inversion of GPS, tilt, and leveling data using a network inversion filter [*Segall and Matthews*, 1997]. The dike opened at a maximum rate of 50 mm/d, had a peak magma flux of 2×10^6 m^3/d, had cumulative dilation of 0.38 m, and migrated slowly upward from ~6 to ~4 km depth [*Aoki et al.*, 1999]. *Cervelli et al.* [2001] applied two Monte Carlo optimization techniques (simulated annealing and random cost) to the same data sets and inferred two sources, a dike and a fault, corresponding to the intrusion and the largest earthquake in the sequence, respectively.

[75] Yet another earthquake swarm occurred in the area during June–July 2000, culminating in an eruption and caldera formation on Miyake Island (also Miyakejima or Miyakejima). Quasiperiodic eruptions had been recorded at Miyakejima since 1085, most recently in 1940, 1962, and 1983. On 26 June 2000, anomalous tilt and an earthquake swarm beneath the island indicated that magma intruded close to the surface, but an eruption did not ensue immediately [*Ukawa et al.*, 2000]. Instead, the swarm migrated toward Kozu Island, 40 km to the northwest, before a small eruption and dramatic subsidence started at Miyakejima on 8 July 2000. A phreatomagmatic eruption on 18 August 2000 was the largest of the sequence, with an eruption column that reached as high as 15 km [*Furuya et al.*, 2003]. The summit depression gradually sank and expanded through mid-August, producing repetitive very long period (VLP) earthquakes and a 1.7-km-diameter caldera [*Nakada et al.*, 2001].

[76] *Kumagai et al.* [2001] proposed a model for caldera formation in which a vertical piston intermittently sinks into the magma reservoir as a result of lateral magma outflow, which accounts for the migration of earthquakes toward Kozu Island. VLP earthquakes occur as the piston intrudes the chamber, causing it to expand. The process is akin to that inferred for large rift

zone intrusions and summit subsidence events at Kilauea Volcano, Hawaii. *Furuya et al*. [2003] proposed a similar model based on repeated gravity, GPS, and photogrammetric surveys. Increasing pressure from the weight of dense cumulate magma eventually causes the reservoir to rupture, resulting in lateral intrusion, a large gravity decrease, and caldera collapse. Groundwater inflow to the magma plumbing system fuels explosive eruptions. Subsequent upwelling of magma causes a large gravity increase, emission of volcanic gases, and volcanic glow, which were observed in that order. Both models are notable for their strong observational constraints.

4.3.2. The 1990–1995 Eruption of Unzen Volcano, Japan

[77] Unzen Volcano (Mount Fugen) reawakened in November 1990 following 198 years of dormancy. After a period of phreatic activity, phreatomagmatic eruptions began in February 1991, followed by extrusion of a dacite dome that started in May 1991 and lasted ~4 years [*Nakada et al*, 1999a]. Virtually all aspects of the activity were very well documented [*Nakada et al*., 1999b], but only the geodetic results are summarized here. Several CGPS stations within 15 km of the vent recorded inflation during the phreatic and phreatomagmatic stages, and deflation following dome growth. The motions were well fit by a Mogi source 6 km west of the vent at 11 km depth, within an aseismic region interpreted as a magma reservoir. For ~1900 days starting no later than December 1989 (~11 months prior to the first phreatic eruption), magma was supplied to the reservoir at an average rate of 1.1×10^5 m^3/d [*Nishi et al*., 1999]. Tiltmeter results that reveal details about the process of magma ascent prior to emergence of the lava dome were discussed in section 3.4 above [*Yamashina and Shimizu*, 1999]. Large, localized deformations during dome growth were analyzed with time-differential stereoscopy, a seldom-used geodetic technique that uses two photographs taken from exactly the same position. Motion of objects in the photos produces a parallax effect that allows visualization of a false stereo image and quantitative analysis of displacements and volume changes [*Yamashina et al*., 1999].

4.4. Lessons From Mount St. Helens, Long Valley, Montserrat, and Japan

[78] Which geodetic techniques have provided the most useful or unanticipated information? Which are the most broadly applicable to a wide range of volcano types and eruptive styles? At Long Valley, frequent measurements (several times per week) of the two-color EDM network have been especially useful for constraining the locations and shapes of various deformation sources and also for tracking temporal changes in the inflation rate. By quickly identifying periods of rapid inflation of the resurgent dome, the two-color data have allowed scientists to anticipate increased earthquake activity beneath the caldera and Mammoth Mountain several weeks in advance [*Hill et al*., 1990]. Unfortunately, two-color EDM technology is not widely used and appears to be fading from the scene. The likely replacement for volcano-monitoring purposes is CGPS, which approaches the two-color EDM in horizontal precision, provides information on surface displacements in three dimensions, and enjoys widespread and growing usage. At Long Valley, 14 CGPS stations were added during 1998–2001 to complement and eventually replace the two-color EDM network. For most applications, CGPS offers compelling advantages over conventional surveying techniques and, with real-time data processing, can also supplement continuous data streams from strain meters and tiltmeters.

[79] Borehole strain meters and the long-base tiltmeter at Long Valley have tracked dome inflation, recorded numerous LP and VLP earthquakes beneath Mammoth Mountain, and helped to document enigmatic, triggered responses to the 1992 M_w 7.3 Landers, California, earthquake [*Hill et al*., 1995] and the 1999 M_w 7.1 Hector Mine, California, earthquake. Short-base tiltmeters in surface installations just a few hundred meters from an active lava dome at Soufriere Hills volcano, Montserrat, recorded repetitive inflation cycles that inspired a general dynamic model for oscillatory behavior at silicic volcanoes [*Voight et al*., 1998, 1999; *Denlinger and Hoblitt*, 1999]. During periods of heightened concern such as earthquake swarms or the aftermath of large earthquakes, only continuously recording sensors such as borehole strain meters, tiltmeters, and CGPS stations with real-time data processing can provide information timely enough to support short-term volcano hazards assessments. Such instruments are therefore essential to a comprehensive volcano-monitoring program.

[80] This point has been made emphatically in Japan, where extensive networks of borehole strain meters, tiltmeters, and CGPS stations have provided an unparalleled record of ground deformation accompanying volcanic activity. The Japanese experience clearly demonstrates the advantage of installing geodetic sensors in relatively deep (100–200 m) boreholes, where extraneous noise is greatly attenuated relative to shallow or surface sites. It is also clear from recent activity at the Izu Peninsula, Unzen, Usu, and elsewhere in Japan that volcano-monitoring programs should be broadly based to capture the full range of phenomena associated with active volcanism. For example, a combination of broadband seismometers, strain meters, and tiltmeters can provide information about ground movements over a wide range in timescales (milliseconds to months), thus helping to merge the fields of volcano seismology and geodesy [*Chouet*, 1996] As a result, geodesists are starting to think about earthquakes as very fast deformation events, while seismologists think about ground deformations as very slow earthquakes. CGPS stations and repeated GPS, leveling, and laser-ranging surveys extend this timescale indefinitely and provide important base-

line information for studies of regional and long-erm deformation.

[81] Repeated leveling surveys offer greater precision for vertical displacements than campaign-style GPS measurements, at least over length scales up to a few tens of kilometers. The combination of precise vertical and horizontal displacements, the former from leveling and the latter from two-color EDM or campaign GPS measurements, provides a powerful constraint on source models that has justified the large investment made in leveling at Long Valley [*Langbein et al*., 1995]. Similarly, leveling data can be combined with microgravity measurements and groundwater information to constrain subsurface mass or density changes, which helps to distinguish among alternative models for surface deformation [*Battaglia et al*., 1999]. For the foreseeable future, leveling will continue to be a valuable supplement to GPS campaigns wherever terrain and available resources allow.

[82] Regional GPS campaigns and InSAR likewise have important roles to play in modern volcano geodesy programs. A well-designed GPS network is in some cases the best means available to capture far-field deformation associated with relatively deep or distributed magmatic sources. For example, *Marshall et al*. [1997] inferred the existence of an inflating dike beneath the Mono Craters chain north of Long Valley caldera on the basis of repeated GPS surveys that spanned a much larger area than other geodetic measurements, which were concentrated within the caldera. InSAR can in many cases provide broad coverage at much greater spatial resolution, and therefore it is preferred for monitoring long-term ground deformation wherever and whenever possible. Unfortunately, InSAR's applicability is limited by heavy vegetation or persistent snow and ice at many volcanoes. The best approach is to combine leveling, GPS, and InSAR surveys to achieve optimal precision and spatial resolution over a broad area, while using continuous sensors (strain meters, tiltmeters, and CGPS) to achieve the desired temporal resolution.

5. CONCLUSIONS AND FUTURE CHALLENGES

[83] Even an ambitious geodetic monitoring program as outlined in sections 3 and 4 would be incomplete without an effective means to combine, analyze, and model various data sets in near real time. There have been important developments in this regard recently [see, e.g., *Owen et al*., 2000; *Segall et al*., 2001] and more seem to be on the horizon. Conceptually, diverse geodetic data sets (e.g., results of GPS, leveling, and microgravity surveys, interferograms, and continuous data streams from borehole tiltmeters, strain meters, and other sensors) need to be combined and weighted according to their relative uncertainties. The appropriate weighting for such diverse model inputs as leveling, GPS, InSAR, and strain meter observations has yet to be completely worked out, but in theory the issue should be a manageable. The weighted data would then be compared to an a priori model that included all known or suspected deformation sources. The model parameters would be optimized by minimizing the misfit between model and data, using some appropriate statistic. Once the model had stabilized, each new piece of geodetic information would be compared to the model's expectations, as defined by predictive filtering or some similar technique, and the model would be updated in near real time. Eventually, the model would converge to a robust "virtual volcano" that could be constantly steered toward reality by automated, real-time data streams. Conversely, the model would identify weaknesses in the monitoring program that could be addressed by new sensors or techniques.

[84] Most deformation models assume that the crust near volcanoes is flat, elastic, and homogeneous, simplifying assumptions that often yield satisfactory results when models are constrained only by relatively limited geodetic data. However, as geodetic measurements become more precise and denser in space and time, the limitations of simple inversion models will likely become apparent. In anticipation of much denser, more precise geodetic data sets in the foreseeable future, more realistic models that include such features as nonidealized source geometry, nonelastic rheology (e.g., viscous or plastic, including temperature and strain rate dependence), and inhomogeneous material properties (e.g., bulk modulus and yield strength) should therefore be developed (T. Masterlark, personal communication, 2001). New geomechanical models based on numerical methods such as finite elements can accommodate such complexities and, if constrained by abundant, high-quality geodetic data in near real time, might produce new insights into active processes near volcanoes.

[85] The network inversion filter [*Segall and Matthews*, 1997; *Aoki et al*., 1999] is an especially promising development in the field of automated, near-real-time deformation modeling. The technique combines elements of linear inverse theory and discrete time Kalman filtering to estimate the distribution of fault slip in space and time using data from dense, frequently sampled geodetic networks. Refinements under development include the addition of other deformation sources that are of interest in volcanology, such as an expanding sphere, ellipsoid, or pipe. In the near future, predictive modeling techniques like the network inversion filter will make it possible to not only track volcano deformation in near real time but also to automatically detect anomalous departures from steady state unrest.

[86] Although fanciful, the system described above does not require any technical breakthroughs in either monitoring or modeling techniques; a prototype could be built relatively quickly with current capabilities. Within the next decade therefore it should be possible to measure and interpret ground deformation at several of the world's volcanoes continuously in near real time. It is

hoped that by learning more about what volcanoes do when they seem to be doing nothing, we will become better equipped to deal with them when lives and property are at risk.

[87] **ACKNOWLEDGMENTS.** This work was supported by the USGS Volcano Hazards Program through the David A. Johnston Cascades Volcano Observatory (CVO) and by the NASA Solid Earth and Natural Hazards Program (SENH) through NASA agreement 19,759. Zhong Lu (USGS, Sioux Falls, South Dakota) and Chuck Wicks (USGS, Menlo Park, California) created Figures 1, 2, and 6. Evelyn Roeloffs and Mike Lisowski (USGS/CVO, Vancouver, Washington) did the numerical modeling depicted in Figures 3 and 4. Steve Schilling and Michelle Howell (USGS/CVO) created Figure 5. Dave Hill (USGS, Menlo Park, California) provided Figures 7–13. Special thanks go to USGS technical reviewers John Power and Zhong Lu and also to Tim Masterlark for his helpful comments on the need for more realistic volcano deformation models. It was a pleasure to fly with helicopter pilot Jeff Linscott of JL Aviation, whose skill and enthusiasm were evident during geodetic surveys at Mount St. Helens and Three Sisters. The author also wishes to thank Yoshimitsu Okada, Paul Segall, and an anonymous reviewer for their thorough and constructive reviews, which included an alternative point of view that is mentioned in the revised text.

[88] Thomas Torgersen was the Editor responsible for this paper. He thanks Paul Segall, Yoshimitsu Okada, and an anonymous reviewer for technical reviews.

REFERENCES

Agustsson, K., R. Stefansson, A. T. Linde, P. Einarsson, I. S. Sacks, G. B. Gudmundsson, and B. Thorbjarndottir, Successful prediction and warning of the 2000 eruption of Hekla based on seismicity and strain changes, *Eos Trans. AGU*, *81*(48), Fall Meet. Suppl., Abstract V11B-30, 2000.

Anderson, J. G., J. N. Brune, J. N. Louie, Y. Zeng, M. Savage, G. Yu, Q. Chen, and D. dePolo, Seismicity in the western Great Basin apparently triggered by the Landers, California, earthquake, 28 June 1992, *Bull. Seismol. Soc. Am.*, *84*, 863–891, 1994.

Aoki, Y., P. Segall, T. Kato, P. Cervelli, and S. Shimada, Imaging magma transport during the 1997 seismic swarm off the Izu Peninsula, Japan, *Science*, *286*, 927–930, 1999.

Battaglia, M., C. Roberts, and P. Segall, Magma intrusion beneath Long Valley Caldera confirmed by temporal changes in gravity, *Science*, *285*, 2119–2122, 1999.

Beauducel, F., P. Briole, and J.-L. Froger, Volcano-wide fringes in ERS synthetic aperture radar interferograms of Etna (1992–1998): Deformation or tropospheric effect?, *J. Geophys. Res.*, *105*, 16,391–16,402, 2000.

Behr, J., R. Bilham, and J. Beavan, Monitoring of magma chamber inflation using a biaxial Michelson tiltmeter in Long Valley Caldera, California, *Eos Trans. AGU*, *73*(43), Fall Meet. Suppl., 347–348, 1992.

Bodin, P., and J. Gomberg, Triggered seismicity and deformation between the Landers, California, and Little Skull Mountain, Nevada, earthquakes, *Bull. Seismol. Soc. Am.*, *84*, 835–843, 1994.

Bonaccorso, A., and P. M. Davis, Models of ground deformation from vertical volcanic conduits with application to eruptions of Mount St. Helens and Mount Etna, *J. Geophys. Res.*, *104*, 10,531–10,542, 1999.

Brantley, S. R., and B. Myers, Mount St. Helens—From the 1980 eruption to 2000, *U.S. Geol. Surv. Fact Sheet*, *036-00*, March 2000.

Casadevall, T. J., The 1989–1990 eruption of Redoubt Volcano, Alaska: Impacts on aircraft operations, *J. Volcanol. Geotherm. Res.*, *62*, 301–316, 1994.

Cervelli, P., M. H. Murray, P. Segall, Y. Aoki, and T. Kato, Estimating source parameters from deformation data, with an application to the March 1997 earthquake swarm off the Izu Peninsula, Japan, *J. Geophys. Res.*, *106*, 11,217–11,237, 2001.

Chouet, B. A., New methods and future trends in seismological volcano monitoring, in *Monitoring and Mitigation of Volcano Hazards*, edited by R., Scarpa and R. I. Tilling, pp. 23–97, Springer-Verlag, New York, 1996.

Chouet, B. A., R. A. Page, C. D. Stephens, J. C. Lahr, and J. A. Power, Precursory swarms of long-period events at Redoubt Volcano (1989–1990), Alaska: Their origin and use as a forecasting tool, *J. Volcanol. Geotherm. Res.*, *62*, 95–135, 1994.

Crandell, D. R., Postglacial lahars from Mount Rainier Volcano, Washington, *U.S. Geol. Surv. Prof. Pap.*, *677*, 75 pp., 1971.

Crandell, D. R., and D. R. Mullineaux, Potential hazards from future eruptions of Mount St. Helens volcano, Washington, *U.S. Geol. Surv. Bull.*, *1383–C*, 26 pp., 1978.

Crandell, D. R., D. R. Mullineaux, and M. Rubin, Mount St. Helens volcano: Recent and future behavior, *Science*, *187*, 438–441, 1975.

Davis, P. M., Surface deformation due to inflation of an arbitrarily oriented triaxial ellipsoidal cavity in an elastic half-space, with reference to Kilauea Volcano, Hawaii, *J. Geophys. Res.*, *91*, 7429–7438, 1986.

Denlinger, R. P., and R. P. Hoblitt, Cyclic eruptive behavior of silicic volcanoes, *Geology*, *27*, 459–462, 1999.

Doroshin, P., Some volcanoes, their eruptions, and earthquakes in the former Russian holdings in America (in Russian), *Zap. Imp. St. Petersb. Mineral. Ova.*, *Ser. 2*, *5*, 25–44, 1870.

Dvorak, J. J., and A. T. Okamura, A hydraulic model to explain variations in summit tilt rate at Kilauea and Mauna Loa Volcanoes, in *Volcanism in Hawaii*, edited by R. W. Decker, T. L. Wright, and P. H. Stauffer, U.S. Geol. Surv. Prof. Pap., *1350*, 1281–1296, 1987.

Dzurisin, D., Geodetic leveling as a tool for studying restless volcanoes and their surroundings, in *Monitoring Volcanoes: Techniques and Strategies Used by the Staff of the Cascades Volcano Observatory, 1980-90*, edited by J., Ewert and D. A. Swanson, *U.S. Geol. Surv. Bull.*, *1966*, 125–134, 1992.

Dzurisin, D., Volcano geodesy: Challenges and opportunities for the 21st century, *Philos. Trans. R. Soc. London*, *Ser. A*, *358*, 1547–1566, 2000.

Dzurisin, D., C. Wicks Jr., and W. Thatcher, Renewed uplift at the Yellowstone Caldera measured by leveling surveys and satellite radar interferometry, *Bull. Volcanol.*, *61*, 349–355, 1999.

Eichelberger, J. C., T. E. C. Keith, T. P. Miller, and C. J. Nye, The 1992 eruptions of Crater Peak vent, Mount Spurr volcano, Alaska: Chronology and summary, *U.S. Geol. Surv. Bull.*, *2139*, 1–18, 1995.

Endo, E., and E. Y. Iwatsubo, Real-time GPS at the Long Valley caldera, California, *Eos Trans. AGU*, *81*(48), Fall Meet. Suppl., Abstract G71C-06, 2000.

Ewart, J. A., B. Voight, and A. Björnsson, Elastic deformation models of Krafla Volcano, Iceland, for the decade 1975 through 1985, *Bull. Volcanol.*, *53*, 436–459, 1991.

Farrar, C. D., M. L. Sorey, W. C. Evans, J. F. Howle, B. D. Kerr, B. M. Kennedy, C.-Y. King, and J. R. Southon, Forest-killing diffuse CO_2 emissions at Mammoth Moun-

tain as a sign of magmatic unrest, *Nature*, *376*, 675–678, 1995.

Fournier, R. O., The transition from hydrostatic to greater than hydrostatic fluid pressure in presently active continental hydrothermal systems in crystalline rock, *Geophys. Res. Lett.*, *18*(5), 955–958, 1991.

Freed, A. M., and J. Lin, Delayed triggering of the 1999 Hector Mine earthquake by viscoelastic stress transfer, *Nature*, *411*, 180–183, 2001.

Fujinawa, Y., S. Shimada, S. Ohmi, S. Sekiguchi, T. Eguchi, and Y. Okada, Fixed point GPS observation of crustal movement associated with the 1989 seismic swarm and submarine volcanic activities off Ito, *J. Phys. Earth*, *39*, 141–153, 1991.

Furuya, M., S. Okubo, W. Sun, Y. Tanaka, J. Oikawa, H. Watanabe, and T. Maekawa, Spatiotemporal gravity changes at Miyakejima volcano, Japan: Caldera collapse, explosive eruptions, and magma movement, *J. Geophys. Res.*, 10.1029/2002JB001989, in press, 2003.

Gerlach, T. M., K. A. McGee, T. Elias, A. J. Sutton, and M. P. Doukas, Carbon dioxide emission rate of Kilauea Volcano: Implications for primary magma and the summit reservoir, *J. Geophys. Res.*, *107*(B9), 2189, 10.1029/2001JB000407, 2002.

Gladwin, M. T., High precision multi component borehole deformation monitoring, *Rev. Sci. Instrum.*, *55*, 2011–2016, 1984.

Gladwin, M. T., and R. Hart, Design parameters for borehole strain instrumentation, *Pure Appl. Geophys.*, *123*(1), 59–80, 1985.

Hill, D. P., Monitoring unrest in a large silicic caldera, the Long Valley-Inyo craters volcanic chain complex in east-central California, *Bull. Volcanol.*, *47*, 371–395, 1984.

Hill, D. P., Temperatures at the base of the seismogenic crust beneath Long Valley caldera, California, and the Phlegraean Fields caldera, Italy, in *Volcanic Seismology*, edited by P. Gasparini, R. Scarpa, and K. Aki, pp. 432–461, Springer-Verlag, New York, 1993.

Hill, D. P., Earthquakes and carbon dioxide beneath Mammoth Mountain, California, *Seismol. Res. Lett.*, *67*, 8–15, 1996.

Hill, D. P., Seismic evidence for a complex magmatic system beneath Long Valley caldera, California, *Seismol. Res. Lett.*, *70*, 222, 1999.

Hill, D. P., and A. M. Pitt, Long period earthquakes at mid-crustal depths beneath the western margin of Long Valley caldera, California, *Eos Trans. AGU*, *73*(43), Fall Meet. Suppl., 343, 1992.

Hill, D. P., W. L. Ellsworth, M. J. S. Johnston, J. O. Langbein, D. H. Oppenheimer, A. M. Pitt, P. A. Reasenberg, M. L. Sorey, and S. R. McNutt, The 1989 earthquake swarm beneath Mammoth Mountain, California: An initial look at the 4 May through 30 September activity, *Bull. Seismol. Soc. Am.*, *80*, 325–339, 1990.

Hill, D. P., et al., Seismicity remotely triggered by the magnitude 7.3 Landers, California, earthquake, *Science*, *260*, 1617–1623, 1993.

Hill, D. P., M. J. S. Johnston, J. O. Langbein, and R. Bilham, Response of Long Valley caldera to the M_w = 7.3 Landers, California, earthquake, *J. Geophys. Res.*, *100*, 12,985–13,005, 1995.

Hill, D. P., et al., Response plan for volcano hazards in the Long Valley caldera and Mono Craters region, California, *U.S. Geol. Surv. Bull.*, *2185*, 57 pp., 2002.

Iwatsubo, E. Y., L. Topinka, and D. A. Swanson, Measurements of slope distances and zenith angles at Newberry and South Sister Volcanoes, Oregon, 1985–1986, *U.S. Geol. Surv. Open File Rep.*, *88-377*, 51 pp., 1988.

Johnston, M. J. S., and R. D. Borcherdt, Earth strain in the period range 0.1–10,000 seconds at six borehole sites within the San Andreas Fault, California, *Eos Trans. AGU*, *65*, 1015, 1984.

Johnston, M. J. S., and A. T. Linde, Implications of crustal strain during conventional, slow, and silent earthquakes, in *International Handbook of Earthquake and Engineering Seismology: Part A, Int. Geophys. Ser.*, vol. 81a, edited by W. H. K. Lee et al., chap. 36, pp. 589–605, Academic, San Diego, Calif., 2002.

Johnston, M. J. S., R. D. Borcherdt, and A. T. Linde, Short-period strain (0.1–10^5 s): Near-source strain field for an earthquake (M_L 3.2) near San Juan Bautista, California, *J. Geophys. Res.*, *91*, 11,497–11,502, 1986.

Johnston, M. J. S., A. T. Linde, and D. C. Agnew, Continuous borehole strain in the San Andreas fault zone before, during, and after the 28 June 1992, M_w 7.3 Landers, California, earthquake, *Bull. Seismol. Soc. Am.*, *84*, 799–805, 1994.

Johnston, M. J. S., D. P. Hill, A. T. Linde, J. Langbein, and R. Bilham, Transient deformation during triggered seismicity from the 28 June 1992, M_W = 7.3 Landers earthquake at Long Valley volcanic caldera, California, *Bull. Seismol. Soc. Am.*, *85*, 787–795, 1995.

Kamo, K., and K. Ishihara, A preliminary experiment on automated judgment of the stages of eruptive activity using tiltmeter records at Sakurajima, Japan, in *Volcanic Hazards: Assessment and Monitoring, IAVCEI Proc. Volcanol.*, vol. 1, edited by J. H. Latter, pp. 585–598, Springer-Verlag, New York, 1989.

Kumagai, H., T. Ohminato, M. Nakano, M. Ooi, A. Kubo, H. Inoue, and J. Oikawa, Very-long-period seismic signals and caldera formation at Miyake Island, Japan, *Science*, *293*, 687–690, 2001.

Lachenbruch, A. H., J. H. Sass, R. J. Munroe, and T. H. Moses Jr., Geothermal setting and simple heat conduction models for the Long Valley caldera, *J. Geophys. Res.*, *81*, 769–784, 1976.

Langbein, J., D. P. Hill, T. N. Parker, and S. K. Wilkinson, An episode of reinflation of the Long Valley caldera, eastern California: 1989–1991, *J. Geophys. Res.*, *98*, 15,851–15,870, 1993.

Langbein, J., D. Dzurisin, G. Marshall, R. Stein, and J. Rundle, Shallow and peripheral volcanic sources of inflation revealed by modeling of two-color geodimeter and leveling data from Long Valley caldera, California, 1988–1992, *J. Geophys. Res.*, *100*, 12,487–12,495, 1995.

Linde, A. T., and I. S. Sacks, Real time predictions of imminent volcanic activity using borehole deformation data, *Eos Trans. AGU*, *81*(48), Fall Meet. Suppl., Abstract V51C-03, 2000.

Linde, A. T., K. Agustsson, I. S. Sacks, and R. Stefansson, Mechanism of the 1991 eruption of Hekla from continuous borehole strain monitoring, *Nature*, *365*, 737–740, 1993.

Linde, A. T., I. S. Sacks, M. J. S. Johnston, D. P. Hill, and R. G. Bilham, Increased pressure from rising bubbles as a mechanism for remotely triggered seismicity, *Nature*, *371*, 408–410, 1994.

Lu, Z., C. Wicks, J. Power, and D. Dzurisin, Ground deformation associated with the March 1996 earthquake swarm at Akutan volcano, Alaska, revealed by satellite radar interferometry, *J. Geophys. Res.*, *105*, 21,483–21,495, 2000a.

Lu, Z., C. Wicks, D. Dzurisin, W. Thatcher, J. T. Freymueller, S. R. McNutt, and D. Mann, Aseismic inflation of Westdahl Volcano, Alaska, revealed by satellite radar interferometry, *Geophys. Res. Lett.*, *27*(11), 1567–1570, 2000b.

Lu, Z., D. Mann, J. Freymueller, D. Meyer, Synthetic aperture radar interferometry of Okmok volcano, Alaska 1: Radar observations, *J. Geophys. Res.*, *105*, 10,791–10,806, 2000c.

Lu, Z., C. Wicks, D. Dzurisin, J. A. Power, S. C. Moran, and W. Thatcher, Magmatic inflation at a dormant stratovol-

cano: 1996–1998 activity at Mount Peulik volcano, Alaska, revealed by satellite radar interferometry, *J. Geophys. Res.*, *107*(B7), 2134, 10.1029/2001JB000471, 2002a.

Lu, Z., J. A. Power, V. S. McConnell, C. Wicks, and D. Dzurisin, Preeruptive inflation and surface interferometric coherence characteristics revealed by satellite radar interferometry at Makushin Volcano, Alaska: 1993–2000, *J. Geophys. Res.*, *107*(B11), 2266, 10.1029/2001JB000970, 2002b.

Marshall, G. A., J. Langbein, R. S. Stein, M. Lisowski, and J. Svarc, Inflation of Long Valley caldera, California, Basin and Range strain, and possible Mono Craters dike opening from 1990-94 GPS surveys, *Geophys. Res. Lett.*, *24*(9), 1003–1006, 1997.

Massonnet, D., and K. L. Feigl, Radar interferometry and its application to changes in the Earth's surface, *Rev. Geophys.*, *36*, 441–500, 1998.

McGee, K. A., and T. M. Gerlach, Annual cycle of magmatic CO_2 in a tree-kill soil at Mammoth Mountain, California: Implications for soil acidification, *Geology*, *26*(5), 463–466, 1998.

McGee, K. A., T. M. Gerlach, R. Kessler, and M. P. Doukas, Geochemical evidence for a magmatic CO_2 degassing event at Mammoth Mountain, California, September–December 1997, *J. Geophys. Res.*, *105*, 8447–8456, 2000.

McTigue, D. F., Elastic stress and deformation near a finite spherical magma body: Resolution of the point source paradox, *J. Geophys. Res.*, *92*, 12,931–12,940, 1987.

Miller, T. P., and B. A. Chouet, The 1989–1990 eruptions of Redoubt Volcano: An introduction, *J. Volcanol. Geotherm. Res.*, *62*, 1–10, 1994.

Miller, T. P., R. G. McGimsey, D. H. Richter, J. R. Riehle, C. J. Nye, M. E. Yount, and J. A. Dumoulin, Catalog of the historically active volcanoes of Alaska, *U.S. Geol. Surv. Open File Rep.*, *98-582*, 104 pp., 1998.

Mogi, K., Relations between the eruptions of various volcanoes and the deformations of the ground surface around them, *Bull. Earthquake Res. Inst. Univ. Tokyo*, *36*, 99–134, 1958.

Moran, S. C., D. R. Zimbelman, and S. D. Malone, A model for the magmatic-hydrothermal system at Mount Rainier, Washington, from seismic and geochemical observations, *Bull. Volcanol.*, *61*, 425–436, 2000.

Nakada, S., H. Shimizu, and K. Ohta, Overview of the 1990–1995 eruption at Unzen Volcano, *J. Volcanol. Geotherm. Res.*, *89*, 1–22, 1999a.

Nakada, S., J. C. Eichelberger, and H. Shimizu (Eds.), Unzen eruption: Magma ascent and dome growth, *J. Volcanol. Geotherm. Res.*, *89*, 315 pp., 1999b.

Nakada, S., M. Nagai, A. Yasuda, T. Shimano, N. Geshi, M. Ohno, T. Akimasa, T. Kaneko, and T. Fujii, Chronology of the Miyakejima 2000 eruption: Characteristics of summit collapsed crater and eruption products (in Japanese with English abstract), *J. Geogr.*, *110*, 168–180, 2001.

Nishi, K., H. Ono, and H. Mori, Global positioning system measurements of ground deformation caused by magma intrusion and lava discharge: The 1990–1995 eruption at Unzendake volcano, Kyushu, Japan, *J. Volcanol. Geotherm. Res.*, *89*, 23–34, 1999.

Okada, Y., Surface deformation due to shear and tensile faults in a half-space, *Bull. Seismol. Soc. Am.*, *75*, 1135–1154, 1985.

Okada, Y., Internal deformation due to shear and tensile faults in a half-space, *Bull. Seismol. Soc. Am.*, *82*, 1018–1040, 1992.

Okada, Y., and E. Yamamoto, A model for the 1989 seismo-volcanic activity off Ito, central Japan, derived from crustal movement data, *J. Phys. Earth*, *39*, 177–195, 1991.

Okada, Y., E. Yamamoto, and T. Ohkubo, Coswarm and preswarm crustal deformation in the eastern Izu Peninsula, central Japan, *J. Geophys. Res.*, *105*, 681–692, 2000.

Oshima, S., M. Tsuchide, S. Kato, S. Okubo, K. Watanabe, K. Kudo, and J. Ossaka, Birth of a submarine volcano "Teisi Knoll," *J. Phys. Earth*, *39*, 1–19, 1991.

Owen, S., P. Segall, M. Lisowski, A. Miklius, M. Murray, M. Bevis, and J. Foster, January 30, 1997 eruptive event on Kilauea Volcano, Hawaii, as monitored by continuous GPS, *Geophys. Res. Lett.*, *27*(17), 2757–2760, 2000.

Pitt, A. M., and D. P. Hill, Long-period earthquakes in the Long Valley caldera region, eastern California, *Geophys. Res. Lett.*, *21*(16), 1679–1682, 1994.

Power, J. A., J. C. Lahr, R. A. Page, B. A. Chouet, C. D. Stephens, D. H. Harlow, T. L. Murray, and J. N. Davies, Seismic evolution of the 1989–1990 eruption sequence of Redoubt Volcano, Alaska, *J. Volcanol. Geotherm. Res.*, *62*, 69–94, 1994.

Power, J. A., A. D. Jolly, R. A. Page, and S. R. McNutt, Seismicity and forecasting of the 1992 eruptions of Crater Peak vent, Mount Spurr volcano: An overview, *U.S. Geol. Surv. Bull.*, *2139*, 149–159, 1995.

Punongbayan, R. S., C. G. Newhall, M. L. P. Bautista, D. Garcia, D. H. Harlow, R. P. Hoblitt, J. P. Sabit, and R. U. Solidum, Eruption hazard assessments and warnings, in *Fire and Mud: Eruptions and Lahars of Mt. Pinatubo, Philippines*, edited by C. G., Newhall and R. S. Punongbayan, pp. 67–85, Univ. of Wash. Press, Seattle, 1996.

Robertson, R. E. A., W. P. Aspinall, R. A. Herd, G. E. Norton, R. S. J. Sparks, and S. R. Young, The 1995–1998 eruption of the Soufriere Hills Volcano, Montserrat, WI, *Philos. Trans. R. Soc. London, Ser. A*, *358*, 1619–1637, 2000.

Sacks, I. S., S. Suyehiro, D. W. Evertson, and Y. Yamagishi, Sacks-Evertson strainmeter, its installation in Japan and some preliminary results concerning strain steps, *Pap. Meteorol. Geophys.*, *22*, 195–207, 1971.

Savage, J. C., and M. M. Clark, Magmatic resurgence in Long Valley caldera, California: Possible cause of the 1980 Mammoth Lakes earthquakes, *Science*, *217*, 531–533, 1982.

Savage, J. C., and R. S. Cockerham, Earthquake swarm in Long Valley caldera, California, January 1983: Evidence for dike inflation, *J. Geophys. Res.*, *89*, 8315–8324, 1984.

Scandone, R., and S. D. Malone, Magma supply, magma discharge and readjustment of the feeding system of Mount St. Helens during 1980, *J. Volcanol. Geotherm. Res.*, *23*, 239–262, 1985.

Segall, P., and M. Matthews, Time dependent inversion of geodetic data, *J. Geophys. Res.*, *102*, 22,391–22,409, 1997.

Segall, P., P. Cervelli, S. Owen, M. Lisowski, and A. Miklius, Constraints on dike propagation from continuous GPS measurements, *J. Geophys. Res.*, *106*, 19,301–19,318, 2001.

Shibata, T., and F. Akita, Precursory changes in well water level prior to the March, 2000 eruption of Usu Volcano, Japan, *Geophys. Res. Lett.*, *28*(9), 1799–1802, 2001.

Shimada, S., Y. Fujinawa, S. Sekiguchi, S. Ohmi, T. Eguchi, and Y. Okada, Detection of a volcanic fracture opening in Japan using Global Positioning System measurements, *Nature*, *343*, 631–633, 1990.

Simkin, T., and L. Siebert, *Volcanoes of the World: A Regional Directory, Gazetteer, and Chronology of Volcanism During the Last 10,000 Years*, 349 pp., Geoscience Press, Tucson, Ariz., 1994.

Simons, M., S. Hensley, M. Murakami, P. A. Rosen, M. Tobita, and F. H. Webb, Observations of crustal deformation in Long Valley, CA using interferometric synthetic aperture radar, *Eos Trans. AGU*, *77*(17), Spring Meet. Suppl., S262, 1996.

Smith, R. B., C. M. Meertens, A. R. Lowry, R. Palmer, and N. M. Ribe, The Yellowstone Hotspot; evolution and its topographic, deformation and earthquake signatures, *Geol. Soc. Am. Abstr. Programs*, *29*, 166, 1997.

Smith, R. B., C. M. Puskas, G. P. Waite, C. M. Meertens, and W. Chang, Tectonic and volcano interaction of the Yellowstone caldera and surrounding faults: Models and deformation budgets from GPS and seismicity measurements, *Eos Trans. AGU*, *80*(46), Fall Meet. Suppl., F970, 1999.

Sorey, M. L., B. M. Kennedy, W. C. Evans, C. D. Farrar, and G. A. Suemnicht, Helium isotope and gas discharge variations associated with crustal unrest in Long Valley caldera, California, *J. Geophys. Res.*, *98*, 15,871–15,889, 1993.

Swanson, D. A., T. J. Casadevall, D. Dzurisin, S. D. Malone, C. G. Newhall, and C. S. Weaver, Predicting eruptions at Mount St. Helens, June 1980 through December 1982, *Science*, *221*, 1369–1376, 1983.

Tait, S., C. Jaupart, and S. Vergniolle, Pressure, gas content and eruption periodicity of a shallow, crystallizing magma chamber, *Earth Planet. Sci. Lett.*, *92*, 107–123, 1989.

Tryggvason, E., Multiple magma reservoirs in a rift zone volcano: Ground deformation and magma transport during the September 1984 eruption of Krafla, Iceland, *J. Volcanol. Geotherm. Res.*, *28*, 1–44, 1986.

Ukawa, M., E. Fujita, E. Yamamoto, Y. Okada, and M. Kikuchi, The 2000 Miyakejima eruption: Crustal deformation and earthquakes observed by the NIED Miyakejima observation network, *Earth Planets Space*, *52*(8), xix–xxvi, 2000.

Voight, B., The management of volcano emergencies: Nevado del Ruiz, in *Monitoring and Mitigation of Volcano Hazards*, edited by R. Scarpa, and R. I. Tilling, pp. 719–769, Springer-Verlag, New York, 1996.

Voight, B., R. P. Hoblitt, A. B. Clarke, A. B. Lockhart, A. D. Miller, L. L. Lynch, and J. McMahon, Remarkable cyclic ground deformation monitored in real time on Montserrat, and its use in eruption forecasting, *Geophys. Res. Lett.*, *25*(18), 3397–3400, 1998.

Voight, B., et al., Magma flow instability and cyclic activity at Soufriere Hills Volcano, Montserrat, British West Indies, *Science*, *283*, 1138–1142, 1999.

Warren, L., D. Gillard, and A. Rubin, Similar long-period earthquakes beneath Kilauea Volcano, *Eos Trans. AGU*, *78*(46), Fall Meet. Suppl., F437–F438, 1997.

White, R. A., and D. Dzurisin, Deep long-period earthquakes: Seismic evidence of rising basalt, *Eos Trans. AGU*, *78*(46), Fall Meet. Suppl., F437, 1997.

Wicks, C. W., Jr., W. R. Thatcher, and D. Dzurisin, Migration of fluids beneath Yellowstone caldera inferred from satellite radar interferometry, *Science*, *282*, 458–462, 1998.

Wicks, C., Jr., D. Dzurisin, S. E. Ingebritsen, W. Thatcher, Z. Lu, and J. Iverson, Magmatic activity beneath the quiescent Three Sisters volcanic center, central Oregon Cascade Range, USA, *Geophys. Res. Lett.*, *29*(7), 1122, 10.1029/2001GL014205, 2002.

Yamamoto, E., Y. Okada, and T. Ohkubo, Ground tilt changes preceding the 1989 submarine eruption off Ito, Izu Peninsula, *J. Phys. Earth*, *39*, 165–176, 1991.

Yamashina, K., and H. Shimizu, Crustal deformation in the mid-May 1991 crisis preceding the extrusion of a dacite lava dome at Unzen volcano, Japan, *J. Volcanol. Geotherm. Res.*, *89*, 43–55, 1999.

Yamashina, K., T. Matsushima, and S. Ohmi, Volcanic deformation at Unzen, Japan, visualized by a time-differential stereoscopy, *J. Volcanol. Geotherm. Res.*, *89*, 73–80, 1999.

Yamashita, K. M., and M. P. Doukas, Precise level lines at Crater Lake, Newberry Crater, and South Sister, Oregon, *U.S. Geol. Surv. Open File Rep.*, 87-293, 32 pp., 1987.

Zebker, H. A., P. A. Rosen, and S. Hensley, Atmospheric effects in interferometric synthetic aperture radar surface deformation and topographic maps, *J. Geophys. Res.*, *102*, 7547–7563, 1997.

Zebker, H. A., F. Amelung, and S. Jonsson, Remote sensing of volcano surface and internal processes using radar interferometry, in *Remote Sensing of Active Volcanism, Geophysical Monograph Ser.*, vol. 116, edited by P. J. Mouginis-Mark, J. A. Crisp, and J. H. Fink, pp. 179–205, AGU, Washington, D. C., 2000.

Zobin, V. M., and V. I. Levina, Rupture history of the January 1, 1996, M_s 6.6 volcanic earthquake preceding the simultaneous eruption of Karymsky and Akademia Nauk volcanoes in Kamchatka, Russia, *J. Geophys. Res.*, *103*, 18,315–18,324, 1998.

D. Dzurisin, David A. Johnston Cascades Volcano Observatory, U.S. Geological Survey, 1300 SE Cardinal Court, Building 10, Suite 100, Vancouver, WA 98683-9589, USA. (dzurisin@usgs.gov)

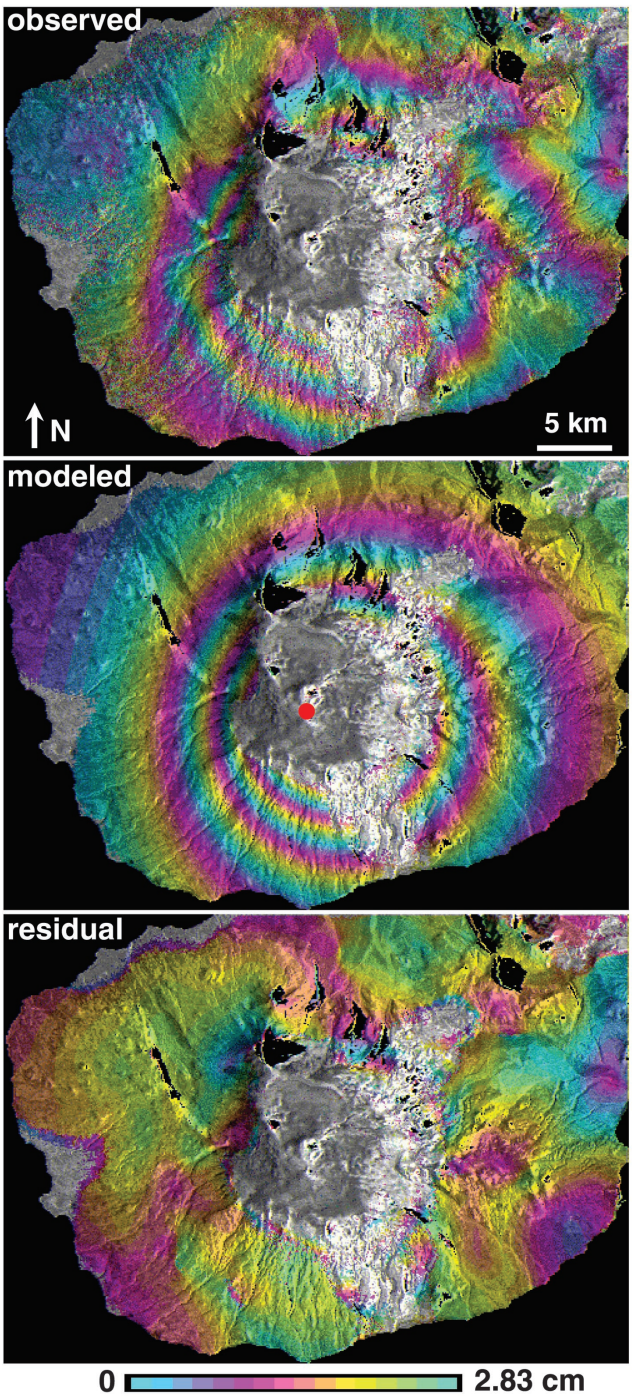

Figure 1. Observed, modeled, and residual interferograms of Westdahl volcano, Alaska, spanning the time interval from 21 September 1993 to 9 October 1998. *Lu et al.* [2000b] produced several such interferograms from pairs of radar images acquired by the European Space Agency's ERS-1 and ERS-2 satellites and a U.S. Geological Survey (USGS) digital elevation model (DEM). Color bands represent interferometric fringes; each full color cycle corresponds to 2.83 cm of range change between the ground and satellite. About three fringes are visible on the volcano's southwest flank. Uncolored area near summit represents permanent ice and snow, where interferometric synthetic aperture radar (InSAR) is ineffective. Extrapolation of the modeled interferogram indicates that the summit moved toward the satellite (i.e., mostly upward because the satellite look angle is ~21° from vertical) ~17 cm during the 5-year observation interval, which did not include any unusual seismicity. *Lu et al.* [2000b] attributed the deformation to magmatic inflation ($\Delta V \approx 0.05$ km^3) of a source ~9 km beneath the center of the volcano (red dot in middle image).

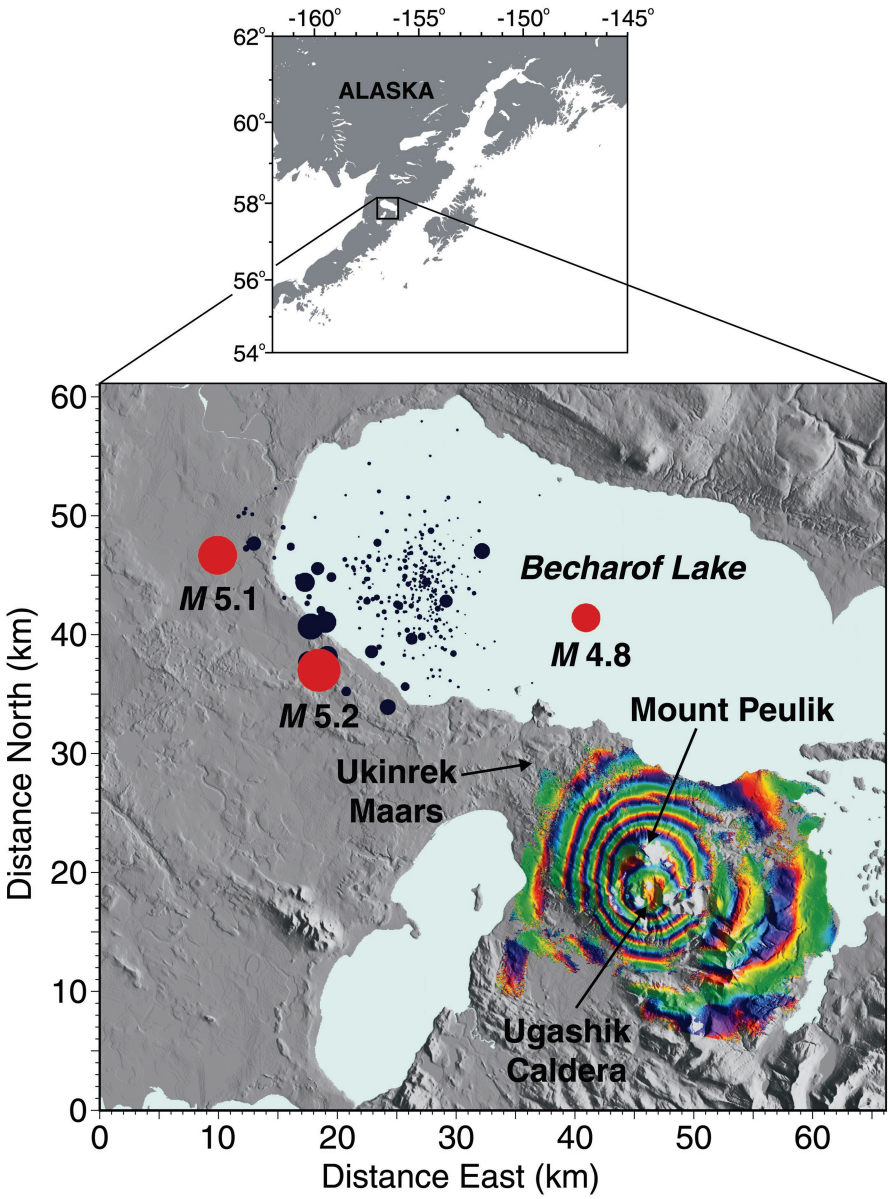

Figure 2. Shaded relief map of the area near Mount Peulik volcano, Alaska, based on the USGS 15-min Alaska DEM. Superimposed on the topography is a radar interferogram for the period from October 1996 to September 1997, showing ~17 cm of inflation centered beneath the volcano's southwest flank. Each interferometric fringe (full color cycle) represents 2.83 cm of range change between the ground and the satellite. Uncolored areas indicate vegetation or other factors that render InSAR ineffective. *Lu et al.* [2002a] used several such interferograms to show that the average inflation rate was ~0.003 km^3/month from October 1996 to September 1997, that it peaked at 0.005 km^3/month from 26 June to 9 October 1997, and that it dropped to 0.001 km^3/month from October 1997 to September 1998. No unusual seismicity was detected beneath the volcano during the inflation episode. However, an intense earthquake swarm occurred ~30 km northwest of Mount Peulik, in the vicinity of the southwest shoreline of Becharof Lake, from May to October 1998. Black ($M < 4.8$) and red ($4.8 \leq M \leq 5.1$) circles represent epicenters of the 1998 swarm. The smallest circles correspond to $M = 0$ and the largest to $M = 5.2$. *Lu et al.* [2002a] modeled the deformation as inflation ($\Delta V = 0.051 \pm 0.005$ km^3) of a magma body located 6.6 ± 0.5 km beneath the southwest flank of Mount Peulik.

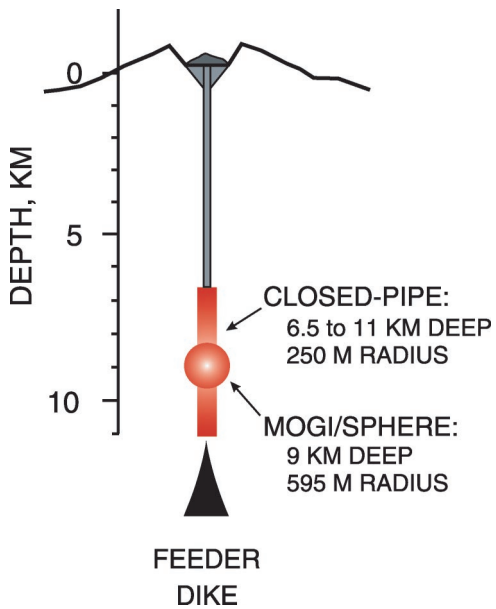

Figure 3. Cross-sectional view of two deformation sources used to model surface deformation: (1) a Mogi source at 9 km depth and (2) a closed pipe extending from 6.5 to 11 km depth. The radii of the sources were chosen to make their volumes equal (V = 0.88 km^3). The surrounding crust was assumed to be elastic and homogeneous. Figure 4 shows calculated surface displacements and strains caused by a volume change of 0.018 km^3 in each source.

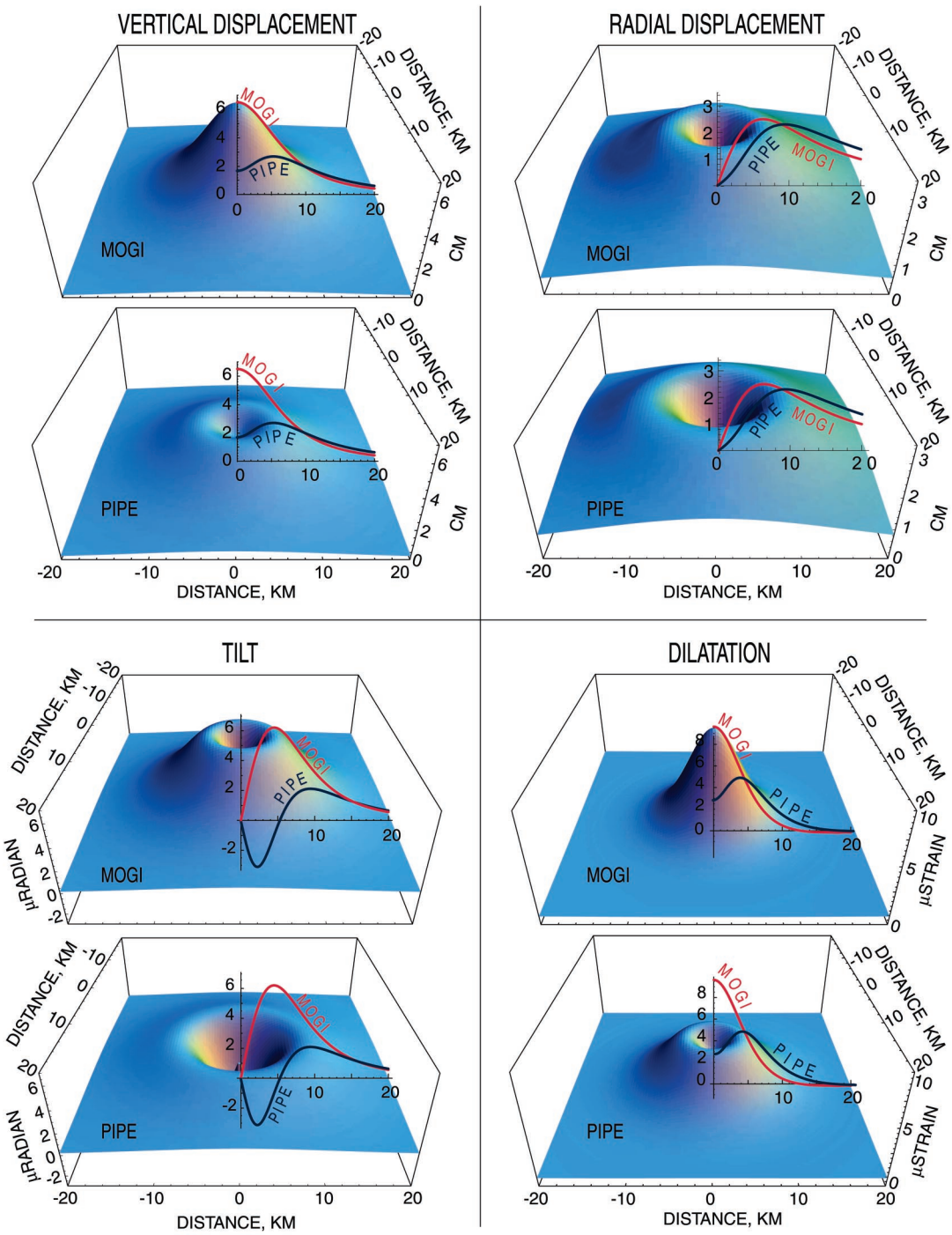

Figure 4. Comparison of model results for a *Mogi* [1958] source centered at 9 km depth and a closed pipe source [*Bonaccorso and Davis*, 1999] between 6.5 and 11 km depth (see Figure 3). Model parameters were chosen to approximate the inferred source for the 18 May 1980 eruption of Mount St. Helens [*Scandone and Malone*, 1985]. Each source has an initial volume of 0.88 km^3 and undergoes a volume increase of 0.018 km^3. Several geodetic sensors at various distances would be required to distinguish between these sources, and the situation would be more complicated if other source geometries were considered (e.g., triaxial ellipsoid, dike, sill, and fault dislocation) or if there were multiple sources, the source depth(s) were not known, or the deformation were not radially symmetric. Numerical modeling and graphic are by E. Roeloffs and M. Lisowski (personal communication, 2001).

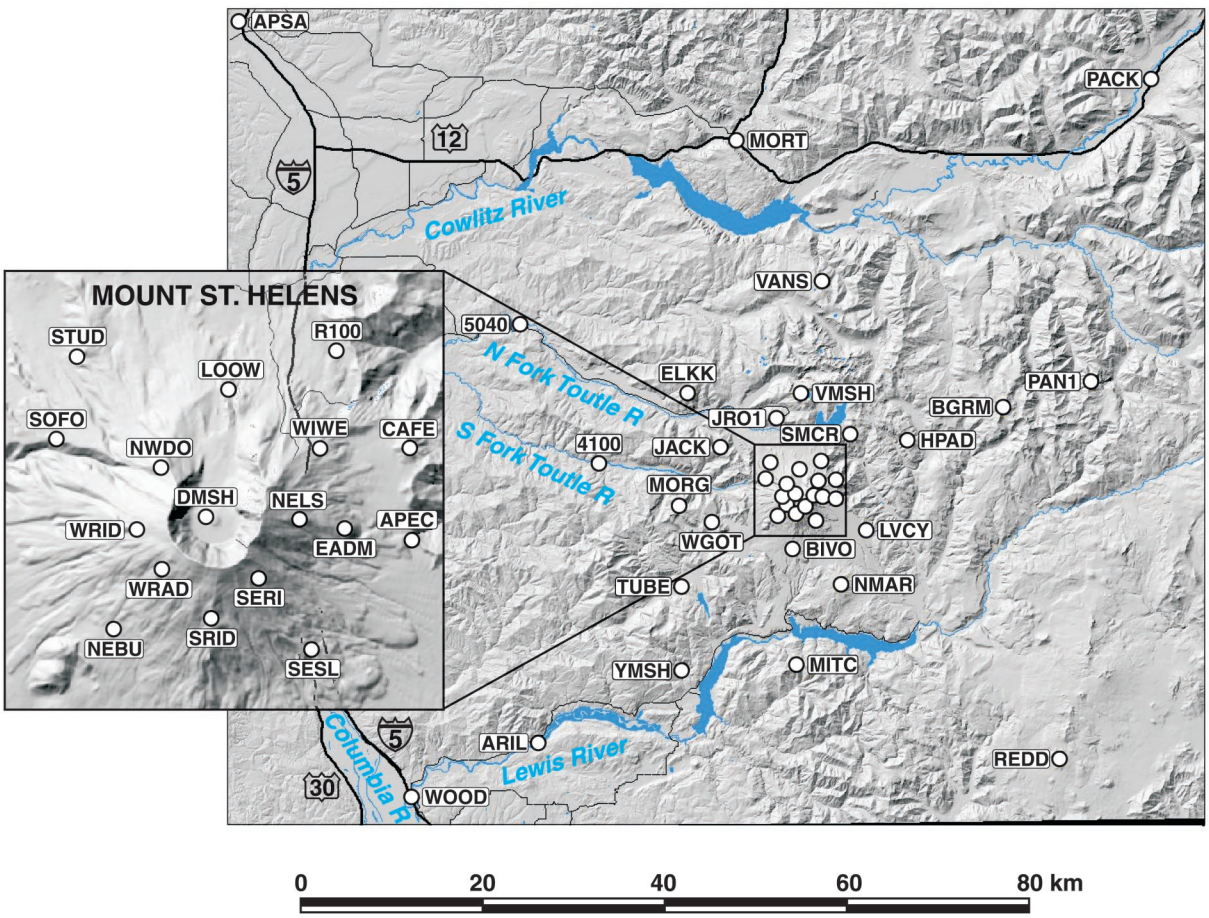

Figure 5. Mount St. Helens large-aperture GPS network, including 40 benchmarks installed and observed during summer 2000, superimposed on a shaded relief version of a USGS digital elevation model. The network is designed to capture both near-field and far-field deformation from magmatic sources near or above the brittle-ductile transition and also tectonic deformation within the St. Helens Seismic Zone. Graphic is by S. Schilling and M. Howell (personal communication, 2001).

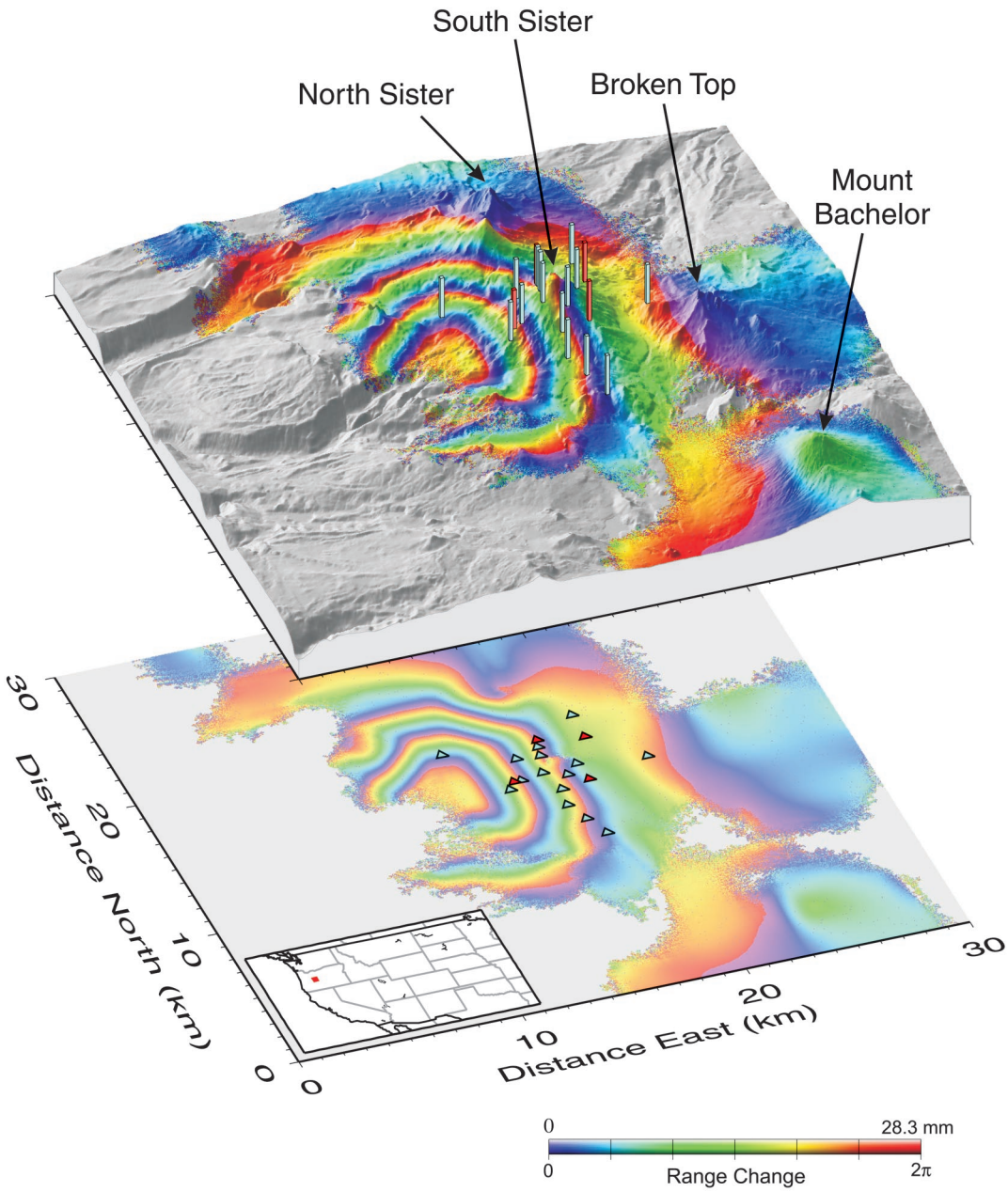

Figure 6. Interferogram of the Three Sisters area, central Oregon Cascade Range, for the period 20 August 1996 to 10 October 2000 [*Wicks et al*., 2002] showing the locations of electronic distance measurement (EDM) benchmarks (cyan bars and triangles) and tilt-leveling benchmark arrays (red bars and triangles) at South Sister. Each interferometric fringe represented by a color band from violet to red represents 2.83 cm of range change from satellite to ground. Approximately four fringes centered 5 km west of South Sister volcano correspond to ~11 cm of surface movement toward the satellite (mostly uplift). The EDM and tilt-leveling networks were established in 1985 and remeasured in 1986 as a baseline to monitor deformation at South Sister [*Iwatsubo et al*., 1988]. They do not extend across the entire deformation field revealed in the interferogram, which illustrates the importance of extending deformation networks well beyond the volcanic edifice to increase the likelihood of capturing far-field or eccentric deformation.

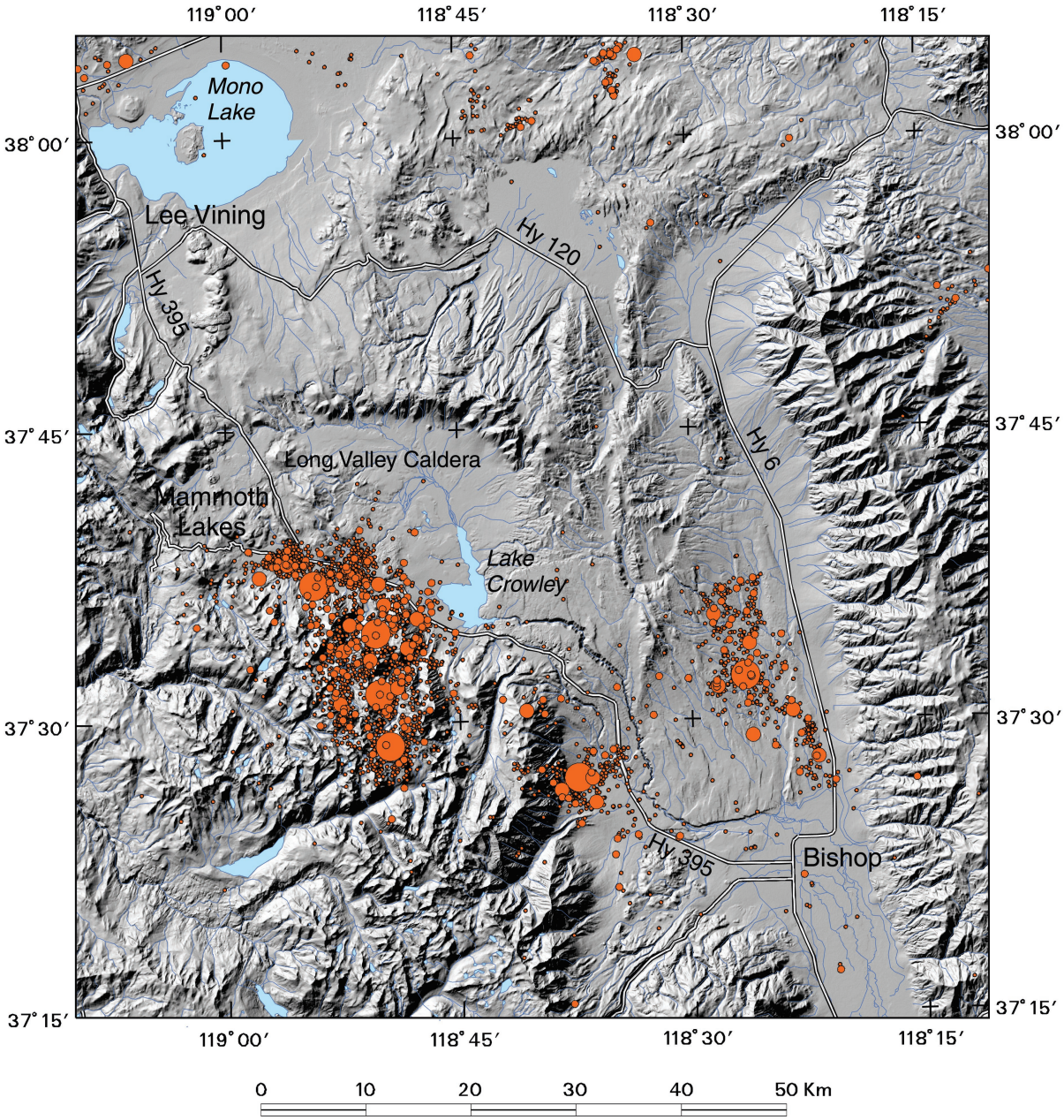

Figure 7. Shaded relief map of the Long Valley region showing epicenters of earthquakes larger than magnitude 3 (circles) for the period 1978–1999 [from *Hill et al.*, 2002]. Largest circles represent events with $5.5 < M < 6.5$. A prolonged episode of unrest began with the M 5.7 Wheeler Crest earthquake on 4 October 1978, midway between the towns of Bishop and Mammoth Lakes. Thereafter sporadic earthquake activity migrated toward the caldera until on 25–27 May 1980 four M 6 events struck beneath the caldera's south moat and adjacent Sierra Nevada block. Subsequent activity has been concentrated in the same area and also beneath Mammoth Mountain, a young cumulovolcano located along the caldera's southwest rim near Mammoth Lakes. The M 6.1 Round Valley earthquake occurred on 23 November 1984, ~10 km NNW of Bishop. Since 1980, ground deformation has been centered at the resurgent dome in the west central part of the caldera, an area that produces very few earthquakes.